

---

# On the Impact of Dataset Properties on Membership Privacy of Deep Learning

---

**Marlon Tobaben**

Department of Computer Science  
University of Helsinki, Finland  
marlon.tobaben@helsinki.fi

**Joonas Jälkö**

Department of Computer Science  
University of Helsinki, Finland  
joonas.jalko@helsinki.fi

**Gauri Pradhan**

Department of Computer Science  
University of Helsinki, Finland  
gauri.pradhan@helsinki.fi

**Yuan He\***

Department of Computer Science  
Aalto University, Finland  
yuan.he@aalto.fi

**Antti Honkela**

Department of Computer Science  
University of Helsinki, Finland  
antti.honkela@helsinki.fi

## Abstract

We apply a state-of-the-art membership inference attack (MIA) to systematically test the practical privacy vulnerability of fine-tuning large image classification models. We focus on understanding the properties of data sets and samples that make them vulnerable to membership inference. In terms of data set properties, we find a strong power law dependence between the number of examples per class in the data and the MIA vulnerability, as measured by true positive rate of the attack at a low false positive rate. We train a linear model to predict true positive rate based on data set properties and observe good fit for MIA vulnerability on unseen data. To analyse the phenomenon theoretically, we reproduce the result on a simplified model of membership inference that behaves similarly to our experimental data. We prove that in this model, the logarithm of the difference of true and false positive rates depends linearly on the logarithm of the number of examples per class. For an individual sample, the gradient norm is predictive of its vulnerability.

## 1 Introduction

Machine learning models are prone to memorising their training data, which makes them vulnerable to privacy attacks such as membership inference attacks (MIAs; Shokri et al., 2017; Carlini et al., 2022) and reconstruction attacks (e.g. Balle et al., 2022; Nasr et al., 2023). Differential privacy (DP; Dwork et al., 2006) provides protection against these attacks, but strong formal protection often comes at the cost of significant loss of model utility.

Finding the correct balance between making models resistant to attacks while maintaining a high utility is important for many applications. In health, for example, many European countries and soon also the EU within the European Health Data Space have requirements that models trained on health data that are made publicly available must be anonymous, i.e. they must not contain information

---

\*Work done while at University of Helsinki.

that can be linked to an identifiable individual. On the other hand, loss of utility of the model due to privacy constraints may compromise the health benefits that might be gained from it.

In this paper, our aim is to apply a state-of-the-art MIA systematically, to help understand practical privacy risks when training deep-learning-based classifiers without DP protections. Our case study focuses on understanding and quantifying factors that influence the vulnerability of non-DP deep learning models to MIA. Since the earliest MIA methods, there has been evidence that classification models with more classes are more vulnerable to MIA (Shokri et al., 2017). Similarly, there is evidence that models trained on fewer samples can be more vulnerable (Chen et al., 2020; Németh et al., 2023). Based on extensive experimental data over many data sets with varying sizes, we uncover a power law describing the vulnerability remarkably well.

Previously, Tobaben et al. (2023) and Yu et al. (2023) have presented limited studies of how data set properties affect the MIA vulnerability. Tobaben et al. (2023) reported how the MIA vulnerability of few-shot image classification is affected by the number of shots (i.e. the number of examples available per class). Yu et al. (2023) studied how the MIA vulnerability of a class in an image classifier trained from scratch depends on the average individual privacy parameters of that class. Our work significantly expands on both of these by more systematic study and modelling of data set properties and by providing a more detailed look at individual samples, not just classes.

**List of contributions** In this work we perform an extensive empirical study on the MIA vulnerability of deep learning models. We focus on a transfer learning setting for image classification tasks, where a large pre-trained neural network is fine-tuned on a sensitive data set, and the MIA is performed on the final classifier. We find that the MIA vulnerability has a strong correlation with certain data set properties (Section 3). In Section 4 we analyse the reasons for these findings more thoroughly and we extend the analysis to individual samples in Section 5. The primary contributions of this work are:

1. *Few-shot MIA*: We conduct a comprehensive study of MIA vulnerability (TPR at fixed low FPR) of target models trained using many different data sets with varying sizes and uncover a power law between the number of examples per class and the vulnerability to MIA (see Figure 1).
2. *Regression model*: We utilise our empirical observations to train a regression model to predict MIA vulnerability ( $\log(\text{TPR} - \text{FPR})$  at fixed low FPR) based on examples per class ( $\log S$ ) and number of classes ( $\log C$ ). We show both very good fit on the training data as well as good prediction quality on unseen data from a different feature extractor and when fine-tuning other parameterisations (see Figure 3).
3. *Theoretical analysis using a simplified model of MIA*: To analyse the phenomenon theoretically, we reproduce the result on a simplified model of membership inference that behaves similarly to our experimental data. In this model we can formally prove that  $\log(\text{TPR} - \text{FPR})$  depends linearly on  $\log S$  (see Section 4).
4. *Individual sample MIA*: We extend the study to individual samples and find: (i) The gradient norm is predictive of vulnerability of an individual sample. (ii) Gradient norms at different stages of learning have different impact, but how depends on the data set (see Section 5).

## 2 Background and Methods

**Notation** for the properties of the training data set  $\mathcal{D}$ : (i)  $C$  for the number of classes (ii)  $S$  for shots (examples per class) (iii)  $|\mathcal{D}|$  for training data set size ( $|\mathcal{D}| = CS$ ). We denote the number of MIA shadow models with  $M$ .

**Membership inference attacks (MIAs)** aim to infer whether a particular sample was part of the training set of the targeted model Shokri et al. (2017). Thus, they can be used to determine lower bounds on the privacy leakage of models to complement the theoretical upper bounds obtained through differential privacy.

**Likelihood Ratio attack (LiRA; Carlini et al., 2022)** While many different MIAs have been proposed Hu et al. (2022), in this work we consider the SOTA: the Likelihood Ratio Attack (LiRA). LiRA assumes an attacker that has black-box access to the attacked model, knows the training data distribution, the training set size, the model architecture, hyperparameters and training algorithm. Based on this information, the attacker can train so-called shadow models (Shokri et al., 2017) which imitate the model under attack but for which the attacker knows the training data set.

LiRA exploits the observation that the loss function value used to train a model is often lower for examples that were part of the training set compared to those that were not. For a target sample  $x$ , LiRA trains the shadow models: (i) with  $x$  as a part of the training set ( $x \in \mathcal{D}$ ) (ii) and without  $x$  in the training set ( $x \notin \mathcal{D}$ ). After training the shadow models,  $x$  is passed through the shadow models, and based on the losses (or predictions) two Gaussian distributions are formed: one for the losses of  $x \in \mathcal{D}$  shadow models, and one for the  $x \notin \mathcal{D}$ . Finally, the attacker computes the loss for the point  $x$  using the model under attack and determines using a likelihood ratio test on the distributions built from the shadow models whether it is more likely that  $x \in \mathcal{D}$  or  $x \notin \mathcal{D}$ . Carlini et al. (2022) proposed an optimisation for performing LiRA for multiple models and points without training a computationally infeasible number of shadow models. We utilise this optimisation.

**Measuring MIA vulnerability** Using the likelihood-ratios from LiRA as a score, we can build a binary classifier to predict whether a sample belongs to the training data or not. The operational characteristics of such classifier can be used to measure the success of the MIA. More specifically, throughout the rest of the paper, we will use the true positive rate (TPR) at a specific false positive rate (FPR) as a measure for the vulnerability. Identifying even a small number of samples with high confidence is considered harmful (Carlini et al., 2022) and thus we focus on the regions of small FPR.

**Measuring the uncertainty for TPR** The TPR values from the LiRA-based classifier can be seen as maximum likelihood-estimators for the probability of producing true positives among the positive samples. Since we have a finite number of samples for our estimation, it is important to estimate the uncertainty in these estimators. Therefore, when we report the TPR values for a single repeat of the learning algorithm, we estimate the stochasticity of the TPR estimate by using Clopper-Pearson intervals Clopper and Pearson (1934). Given TP true positives among P positives, the  $1 - \alpha$  confidence Clopper-Pearson interval for the TPR is given as

$$\begin{aligned} B(\alpha/2; TP, P - TP + 1) &< TPR \\ TPR &< B(1 - \alpha/2; TP + 1, P - TP), \end{aligned} \tag{1}$$

where  $B(q; a, b)$  is the  $q$ th-quantile of Beta( $a, b$ ) distribution.

### 3 MIA Vulnerability and Data Set Properties

In this section, we investigate how different properties of data sets affect the MIA vulnerability. Based on our observations, we propose a method to predict the vulnerability to MIA using these properties.

#### 3.1 Experimental Setup

We focus on a image classification setting where we fine-tune pre-trained models on sensitive downstream data sets and assess the MIA vulnerability using LiRA with  $M = 256$  shadow models. We base our experiments on a subset of the few-shot benchmark VTAB (Zhai et al., 2019) that achieves a test classification accuracy  $> 80\%$  (see Table A2).

We report results for fine-tuning a last layer classifier (Head) trained on top of a Vision Transformer ViT-Base-16 (ViT-B; Dosovitskiy et al., 2021), pre-trained on ImageNet-21k Russakovsky et al. (2015). The results for using ResNet-50 (R-50; Kolesnikov et al., 2020) as a backbone can be found in Appendix B.1. We optimise the hyperparameters (batch size, learning rate and number of epochs) using the library Optuna Akiba et al. (2019) with the Tree-structured Parzen Estimator (TPE; Bergstra et al., 2011) sampler with 20 iterations (more details in Appendix A.2). We provide the the code for reproducing the experiments in the supplementary material.

#### 3.2 Experimental Results

Using the setting described above, we study how the number of classes and the number of shots affect the vulnerability (TPR at FPR as described in Section 2). We make the following observations:

- A larger number of  $S$  (**shots**) decrease the vulnerability in a power law relation as demonstrated in Figure 1a. We provide further evidence of this in the Appendix (Figure A.1 and Tables A3 and A4).
- Contrary, a larger number of  $C$  (**classes**) increases the vulnerability as demonstrated in Figure 1b with further evidence in Figure A.2 and Tables A5 and A6 in the Appendix. However, the trend w.r.t.  $C$  is not as clear as with  $S$ .

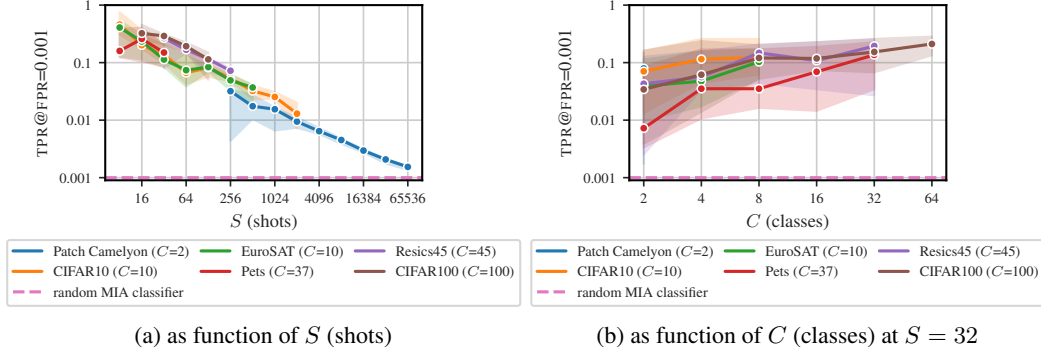


Figure 1: MIA vulnerability (TPR at FPR = 0.001) as a function of data set properties when attacking a ViT-B Head fine-tuned without DP on different data sets. The solid line displays the median and the error bars the minimum of the lower bounds and maximum of the upper bounds for the Clopper-Pearson CIs over multiple seeds (six for Figure 1a and 12 for Figure 1b)

### 3.3 Model to Predict Data Set Vulnerability

The trends seen in Figure 1 suggest a linear dependence of  $\log$  TPR on  $\log S$ . In order to encode the knowledge that  $\text{TPR} > \text{FPR}$ , we modify the model slightly and fit a linear regression model to predict  $\log(\text{TPR} - \text{FPR})$  for each  $\text{FPR} = 10^{-k}$ ,  $k = 1, \dots, 5$  separately using the  $\log C$  and  $\log S$  as covariates with statsmodels (Seabold and Perktold, 2010). The general form of the model can be found in Equation (2), where  $\beta_S, \beta_C$  and  $\beta_0$  are the learnable regression parameters.

$$\log_{10}(\text{TPR} - \text{FPR}) = \beta_S \log_{10}(S) + \beta_C \log_{10}(C) + \beta_0 \quad (2)$$

In Appendix B.2, we propose a variation of the regression model that predicts  $\log_{10}(\text{TPR})$  instead of  $\log_{10}(\text{TPR} - \text{FPR})$  but this alternative model performs worse on our empirical data and predicts  $\text{TPR} < \text{FPR}$  in the tail when  $S$  is very large.

We use MIA results of ViT-B (see Table A3) as the training data. Based on the  $R^2$  (coefficient of determination) score ( $R^2 = 0.930$  for the model trained on  $\text{FPR} = 0.001$  data), our model fits the data extremely well. We provide further evidence for other FPR in Figure A.3 and Table A8 in the Appendix. Figure 2 shows the parameters of the prediction model fitted to the training data.

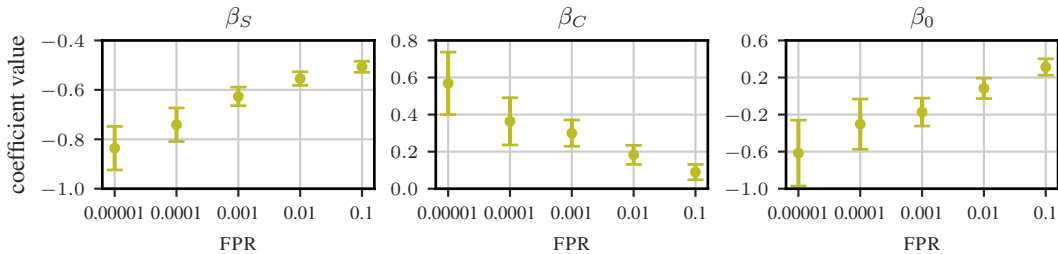


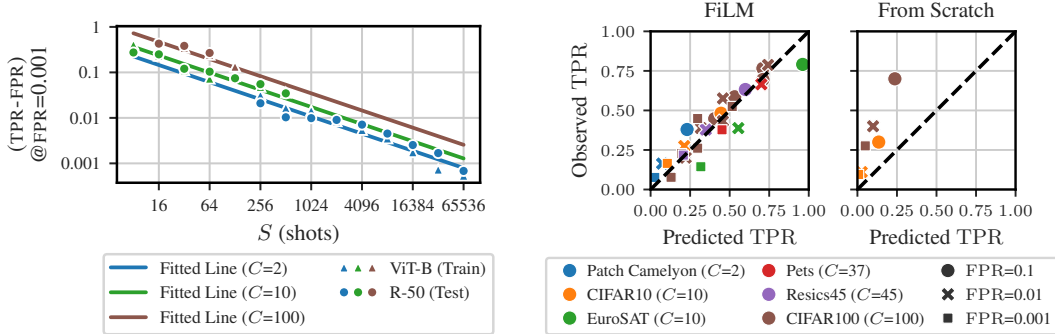
Figure 2: Coefficient values for different FPR when fitting a regression model based on Equation (2) fitted on data from ViT-B (Head) (Table A3). The error bars display the 95% confidence intervals based on Student’s t-distribution.

**Prediction quality on other MIA target models** We analyse how the regression model trained on the ViT-B (Head) data generalizes to other target models. The main points are:

- *R-50 (Head)*: Figure 3a shows that the regression model is robust to a change of the feature extractor, as it is able to predict the TPR for R-50 (Head) (test  $R^2 = 0.790$ ).
- *R-50 (FiLM)*: Figure 3b shows that the prediction quality is good for R-50 (FiLM) models. These models are fine-tuned with parameter-efficient FiLM (Perez et al., 2018) layers (See Appendix A.1). Tobaben et al. (2023) demonstrated that FiLM layers are a competitive alternative to training all

parameters. We supplement the MIA results of Tobaben et al. (2023) with own FiLM training runs. Refer to Table A7 in the Appendix.

- *From-Scratch-Training*: Carlini et al. (2022) provide limited results on from-scratch-training. To the best of our knowledge these are the only published LiRA results on image classification models. Figure 3b displays that our prediction model underestimates the vulnerability of the from-scratch trained target models. We have identified two potential explanations for this (i) In from-scratch-training all weights of the model need to be trained from the sensitive data and thus potentially from-scratch-training could be more vulnerable than fine-tuning. (ii) The strongest attack in Carlini et al. (2022) uses data augmentations to improve the performance. We are not using this optimization.



(a) Predicted MIA vulnerability ((TPR - FPR) at FPR = 0.001) as a function of  $S$  (shots). The dots show the median TPR for the train set (ViT-B; Table A3) and the test set (R-50; Table A4) over six seeds (data sets: Patch Camelyon, EuroSAT and CIFAR100).

(b) Evaluating prediction performance for target models (i) left: fine-tuned with FiLM (data partially from Tobaben et al. (2023), see Table A7) (ii) right: trained from scratch (data from Carlini et al. (2022))

Figure 3: Performance of the regression model based on Equation (2) fitted on data from Table A3.

## 4 Understanding the MIA Prediction Model

In this section, we focus on understanding why the previously observed trends exist. Our goal is to formally prove a similar relationship as in the predictive model of Section 3.3.

### 4.1 A Simplified Model of Membership Inference

In this section, we construct a simplified model of membership inference that streamlines the data generation and shadow model training. We observe that the trends of the vulnerability of the simplified model is a good approximation of the trends previously observed with the image classification example.

Instead of training linear classifiers to classify images, we sample vectors on a high dimensional unit sphere and classify based on inner product with estimated class mean. This model is easier to analyse theoretically, and allows us to simulate arbitrary combinations of  $S$  and  $C$  without relying on the existence of a specific image classification downstream data set as especially high  $C$  image classification downstream data sets that are computationally feasible to fine-tune on have small  $S$ . We generate the data and form the classifiers (which are our target models) as follows:

1. For each class, we first sample a true class mean  $m_c$  on a high dimensional unit sphere that is orthogonal to all other true class means ( $\forall i, j \in C : m_i \perp m_j \vee i = j$ ).
2. We sample  $2S$  vectors  $x_c$  for each class. We assume that they are Gaussian distributed around the true class mean  $x_c \sim \mathcal{N}(m_c, s^2 I)$  where the  $s^2$  is the in-class variance.
3. For each "target model" we randomly choose a subset of size  $CS$  from all generated vectors and compute per-class means  $r_c$ .

- The computed mean is used to classify sample  $(x, y)$  by computing the inner product  $\langle x, r_c \rangle$  as a metric of similarity.

The attacker has to infer which vectors have been used for training the classifier. Instead of utilising the logits (like in the image classification example), the attacker can use the inner products of a point with the cluster means. In Figure 4 we compare the attacker’s performance as a function of  $C$  and  $S$  to the the previous image classification example.

This simplified model resembles the linear (Head) classifier. In the linear classifier, we find a matrix  $A$  and biases  $b$ , to optimize the cross-entropy between the labels and logits  $Az + b$ , where  $z$  denotes the feature space representation of the data. In the simplified model, the rows of  $A$  are replaced by the cluster means and we do not include the bias term in the classification.

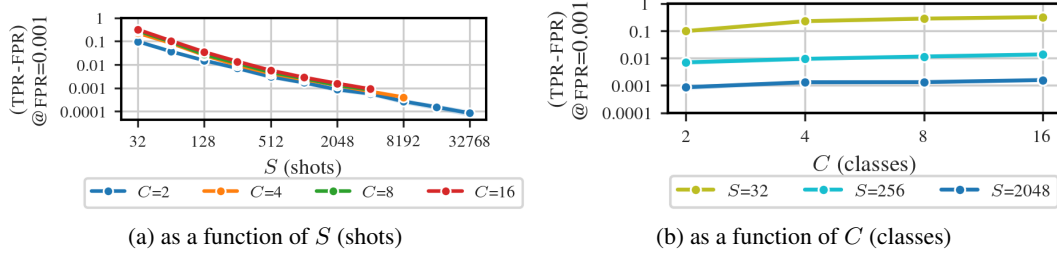


Figure 4: Observed (TPR - FPR) at FPR = 0.001 for the simplified model with in-class  $\sigma = 0.1$ .

## 4.2 Theoretical Analysis

Similarly to the setting in Section 4.1, we focus on a classification model that aims to classify the sample  $(x, y)$  based on the inner product  $\langle x, r_c \rangle$ , where  $r_c$  is the mean of the training data points  $x_m$  with  $y_m = c$ . However, we only focus on the scores of the target class, i.e.  $c = y$ , and therefore the score used of LiRA simplifies to  $\langle x, r_y \rangle$ .

The FPR for LiRA is given as

$$\text{FPR} = \Pr \left( \frac{\mathcal{N}(t_x; \mu_{\text{in}}, \sigma_{\text{in}}^2)}{\mathcal{N}(t_x; \mu_{\text{out}}, \sigma_{\text{out}}^2)} > \exp(\tau) \mid x \notin \mathcal{D}_{\text{target}} \right), \quad (3)$$

where  $t_x = \langle x, r_y^{(\text{target})} \rangle$  is the score for the target model,  $\tau$  is the decision threshold for the classifier, and  $\mu_{\text{in}}, \mu_{\text{out}}, \sigma_{\text{in}}$  and  $\sigma_{\text{out}}$  are the LiRA statistics computed from the shadow models. We assume that  $\sigma_{\text{in}} = \sigma_{\text{out}} = \sigma$ , which allows to write Equation (3) as

$$\text{FPR} = \Pr \left( \log \frac{\mathcal{N}(t_x; \mu_{\text{in}}, \sigma^2)}{\mathcal{N}(t_x; \mu_{\text{out}}, \sigma^2)} > \tau \mid x \notin \mathcal{D}_{\text{target}} \right) \quad (4)$$

$$= \Pr \left( -\frac{1}{2\sigma^2} (\mu_{\text{in}} - \mu_{\text{out}}) [-2t_x + (\mu_{\text{in}} + \mu_{\text{out}})] > \tau \mid x \notin \mathcal{D}_{\text{target}} \right). \quad (5)$$

From now on, we will denote the  $-\frac{1}{2\sigma^2} (\mu_{\text{in}} - \mu_{\text{out}}) [-2t_x + (\mu_{\text{in}} + \mu_{\text{out}})]$  with  $\lambda_{\text{FPR}}$  when  $x \notin \mathcal{D}_{\text{target}}$  and with  $\lambda_{\text{TPR}}$  otherwise. Furthermore we will drop the condition  $x \in \mathcal{D}_{\text{target}}$  or  $x \notin \mathcal{D}_{\text{target}}$  from the FPR and TPR expressions

$$\text{FPR} := \Pr(\lambda_{\text{FPR}} > \tau) \quad (6)$$

$$\text{TPR} := \Pr(\lambda_{\text{TPR}} > \tau). \quad (7)$$

**Lemma 1.** *In the limit of infinite shadow models and with large enough  $S$ , the LiRA test statistics  $\lambda_{\text{FPR}}$  and  $\lambda_{\text{TPR}}$  obtain the following forms*

$$\lambda_{\text{FPR}} = -\frac{1}{2s^2 \|x\|^2} \langle x, x - m_y \rangle \left( \frac{2s}{\sqrt{S}} \langle x, z \rangle + \frac{1}{S} \langle x, x - m_y \rangle \right) \quad (8)$$

$$\lambda_{\text{TPR}} \approx -\frac{1}{2s^2 \|x\|^2} \langle x, x - m_y \rangle \left( \frac{2s}{\sqrt{S}} \langle x, z \rangle - \frac{2}{S} \|x\|^2 + \frac{1}{S} \langle x, x - m_y \rangle \right), \quad (9)$$

where  $z \sim \mathcal{N}(0, I_d)$ .

*Proof.* We defer the proof to Appendix C.  $\square$

The factors independent of  $S$  in for both  $\lambda_{\text{FPR}}$  and  $\lambda_{\text{TPR}}$  correspond to the  $-(\mu_{\text{in}} - \mu_{\text{out}})/(2\sigma^2)$ . Figure A.5 illustrates how this factor behaves as a function of  $S$  in our experiments with the simple model. As predicted by the theory, the factor (i.e. the difference in means divided by the variance) remains fairly constant across different values of  $S$ .

Using Lemma 1 we can derive a rate for the decision threshold  $\tau$ :

**Corollary 2.** *In order to maintain constant FPR, we need to adjust  $\tau$  as  $O(1/\sqrt{S})$ .*

According to Corollary 2, the  $\tau := \tau(S)$  evolves as  $O(1/\sqrt{S})$ , and we will approximate it as  $\tau(S) = \gamma_1 \frac{1}{\sqrt{S}}$ , with constant  $\gamma_1$  depending on the target FPR.

**Theorem 3.**  *$\log(\text{TPR} - \text{FPR})$  depends linearly on  $\log(S)$ .*

*Proof.* From Lemma 1, we see that  $\lambda_{\text{FPR}}$  and  $\lambda_{\text{TPR}}$  differ only in a single term which evolves as  $O(1/S)$ . Thus for sufficiently large  $S$  we can consider this additional r.v. as a small constant shift to the distribution of  $\lambda_{\text{FPR}}$ . Let us denote this variable now with  $q$ . When  $S$  grows,  $q$  becomes small, and we have

$$\text{TPR} - \text{FPR} = \Pr(\lambda_{\text{FPR}} > \tau - q) - \Pr(\lambda_{\text{FPR}} > \tau) \quad (10)$$

$$\approx p_{\lambda_{\text{FPR}}}(\tau)q. \quad (11)$$

Taking the log yields

$$\log(\text{TPR} - \text{FPR}) \approx \log(p_{\lambda_{\text{FPR}}}(\tau)) + \log q \quad (12)$$

$$= \log(p_{\lambda_{\text{FPR}}}(\tau)) - \log S + \gamma_2. \quad (13)$$

From Lemma 1, we can see that a scaled r.v.  $\hat{\lambda}_{\text{FPR}} := \sqrt{S}\lambda_{\text{FPR}}$  becomes almost independent of  $S$  for large enough  $S$ . Hence using the change of variables formula, we have that  $p_{\lambda_{\text{FPR}}}(t) = p_{\hat{\lambda}_{\text{FPR}}}(\sqrt{S}t)\sqrt{S}$ . Now, evaluating  $p_{\lambda_{\text{FPR}}}(t)$  at  $t = \tau(S)$ , we get  $p_{\lambda_{\text{FPR}}}(t) = p_{\hat{\lambda}_{\text{FPR}}}(\gamma_1)\sqrt{S}$ , where the  $p_{\hat{\lambda}_{\text{FPR}}}(\gamma_1)$  is independent of  $S$ . Therefore, ignoring additive constants,

$$\log(\text{TPR} - \text{FPR}) \approx \log \sqrt{S} - \log S = \frac{1}{2} \log S - \log S = -\frac{1}{2} \log S. \quad (14)$$

This shows that  $\log(\text{TPR} - \text{FPR})$  depends linearly on  $\log S$ .  $\square$

Compared to the model in Section 3.3, our theoretical model predicts  $\beta_S = -1/2$ . Our empirical estimates match this for high FPR. For lower FPR,  $\beta_S$  decreases, which indicates there may be finer details of  $p_{\lambda_{\text{FPR}}}$  we are missing in this analysis.

## 5 MIA Vulnerability For Data Samples

This section extends our investigation from the data-set-level properties (Section 3) to individual data-sample-level properties. Previously Yu et al. (2023) have studied correlations between classes and privacy risk before, but in comparison to their study, we look at data samples independent from classes. We investigate two properties that could potentially influence the vulnerability of data points:

- **Per-sample gradients:** Per-sample gradients form the basis for DP individual accounting (Feldman and Zrnic, 2021; Koskela et al., 2023). Under individual Gaussian DP (GDP, Dong et al., 2022) accounting (Koskela et al., 2023), the cumulative  $\mu$ -GDP privacy loss of individual  $i$  with individual gradient norms  $g_{i,t}$  is  $\mu_{i,\text{tot}} \propto \sqrt{\sum_t g_{i,t}^2}$ . Our hypothesis is that this similarly holds also for MIA vulnerability in non-DP settings.
- **Feature space distances:** The pre-trained feature extractors project images into a feature space in which one can compute distances between individual data samples. Our hypothesis is that data samples that are further away from other data samples are easier to distinguish.

## 5.1 Experimental Setup

Our model training is done as in Section 3.1. The target models are fine-tuned pre-trained ViT-B (Head) and R-50 (Head) models. Below we describe how we measure the sample properties and individual TPR at FPR.

**Recording of gradient norms** During the training of the target models we record the per-sample gradient norm for every sample at every step (independent of being part of the current batch) efficiently using Opacus (Yousefpour et al., 2021). The recording of the gradient norms is identical to the DP individual accounting, with the exception that we record the gradient norms of out-samples as well. In our analysis, we are utilising the square root of the sum of squared gradient norm per sample over deciles of steps (i.e. the sum of squared individual gradient norms over the first 10% of steps, second 10% of steps, ..., last 10% of steps).

$$G_i^{(\alpha)} = \sqrt{\sum_{t=\lfloor T(\alpha-0.1) \rfloor}^{\lfloor T\alpha \rfloor} g_{i,t}^2}, \alpha = (0.1, 0.2, \dots, 1.0) \quad (15)$$

**Computation of distance in feature space** All samples are projected into a feature space using the pre-trained model. We measure the Euclidean distance of all examples (in and out) to all in-samples in the feature space and report the distance to the nearest in-sample.

**TPR at FPR for individual samples** We study individual samples, but aggregate the results over multiple data samples by binning the samples based on their data sample properties to reduce the noise. For each data sample we compute its property and assign the sample to a bin based on its percentile in relation to other samples. We then compute the TPR at FPR for each bin. We finally report for each data property bin the percentile of the TPR at FPR.

Throughout our experiments we noticed that the amount of data points needs to be sufficiently large, in order to allow for an appropriate estimation of the TPR at FPR. Thus, we use a sufficient amount of shots ( $S$ ) so that the size of in- and out-set combined is at least  $2|\mathcal{D}| = 1000$  (see Table A10).

## 5.2 Individual Gradient Norms Are Predictive of Individual MIA Vulnerability

Figure 5 shows the observed relationships between the MIA vulnerability and the average individual gradient norms at  $FPR = 0.001$ . When plotting the data for all deciles of steps at once, we find that the average gradient norms are correlated with the vulnerability in all our experiments, but the strength of the correlation depends on the data set. The  $R^2$  (coefficient of determination) compares the observed relationship to a scenario where individual gradient norms would be a perfect predictor (corresponding to a scenario where all points are on the diagonal line). See more results in Table A10 and Figure A.6 in the Appendix.

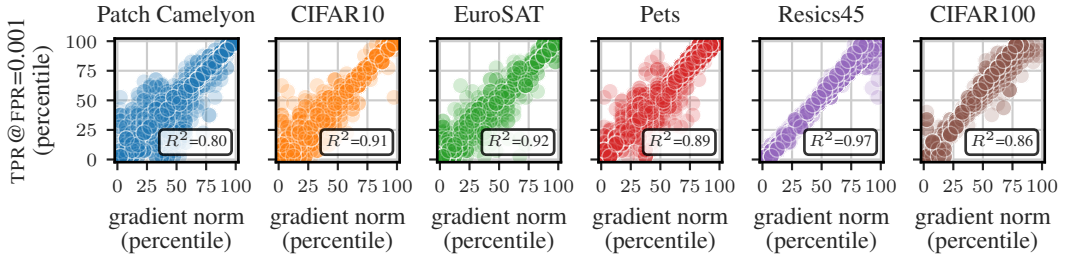


Figure 5: MIA vulnerability (TPR at FPR; percentiles among a seed) as a function of individual gradient norms (binned among a seed). Data obtained over six seeds. The  $R^2$  score compares the observed relationship to a scenario where individual gradient norms would be a perfect predictor.

**Which parts of the training are more predictive?** In Figure 6, we examine whether the gradient norms at different stages of training are a better predictor of vulnerability by computing the ratio between the  $R^2$  per iteration decile and  $R^2$  over the whole training. For most data sets the ratio is constantly at a value of roughly 1, which suggests that gradient norms over even short segments can be as predictive as the norms of the whole trace.

Furthermore, there are deviations that indicate that for some data sets, gradient norms during the early iterations can be relatively more predictive than the norms of the entire trace. This is interesting, as the DP bound would directly depend on the norms of the entire trace.

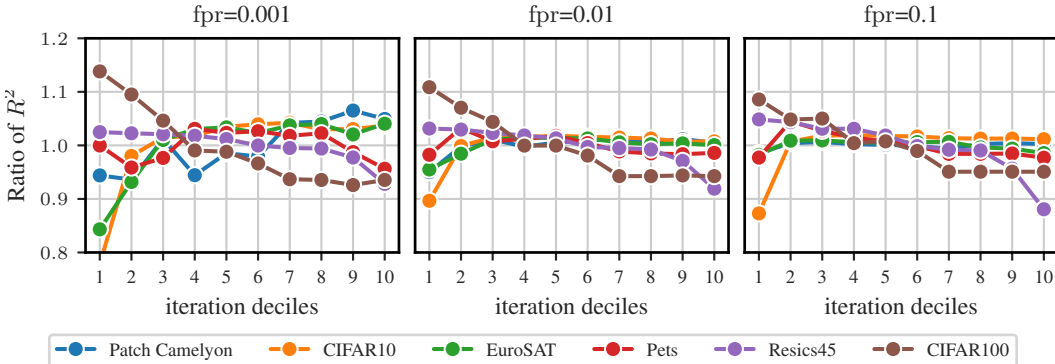


Figure 6: Ratio between  $R^2$  per iteration decile and  $R^2$  over the whole training. A ratio  $> 1$  means that the decile is as more predictive than whole trace and a ratio  $< 1$  means that it is less predictive.

### 5.3 Distance to Neighbors in Feature Space of Pre-trained Model

Figure 7 shows the observed relationships between the MIA vulnerability and distance to the nearest neighbor in the feature space. The distance of data samples to their nearest neighbor correlates with the vulnerability all analysed data sets but Patch Camelyon and Resics45. The observation holds over all FPR and for R-50 (Head) as well, refer to Figures A.9 and A.10 in the Appendix.

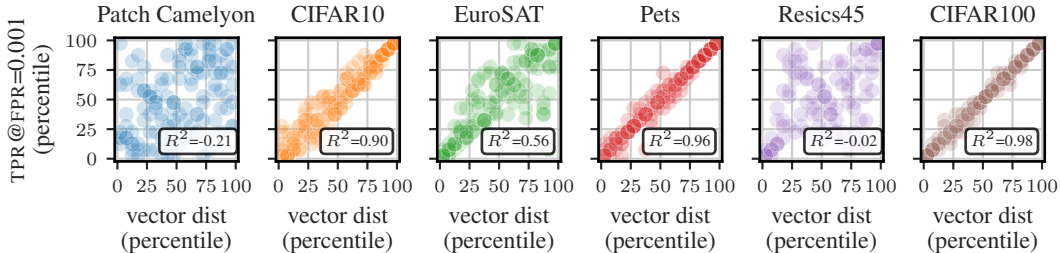


Figure 7: MIA vulnerability (TPR at FPR; percentiles among a seed) as a function of feature space distance (binned among a seed). The results have been obtained over six seeds.

## 6 Discussion

Under the GDPR and similar legal regimes, machine learning (ML) models trained on personal data that memorise the data are personal data and need to be carefully protected. Our work analyses in which cases trained models would most likely be personal data and in which cases they might not be. This will help in evaluating the risk of different kinds of models, favouring less risky models when possible and paying extra attention to more risky cases.

As the best means of protecting privacy, DP, reduces the utility of models, it is important to understand when it is necessary. Our results highlight that models are most vulnerable to MIA when the number of examples per class is low. This leads to an unfortunate dilemma: DP seems most important in the regime where it likely reduces the model utility the most.

Our model singles out the number of examples per class  $S$  as the key predictor of model vulnerability. While our results are based on balanced data sets, it seems likely that minority classes and outliers would be more vulnerable as predicted by our model given their smaller  $S$ . Studying the vulnerability in unbalanced data and in the presence of outliers is an important area of future work.

**Limitations** Our work measures the vulnerability through running one particular MIA. There is no guarantee that models that are not vulnerable to this attack might not be vulnerable to some stronger attack. Formal bounds on attack susceptibility would require something like DP.

Due to computational constraints, our predictive model is based only on transfer learning with fine-tuning only a part of the model. Limited comparison of our model predictions to previous results indicates it may underestimate their vulnerability.

**Broader Impact** Our work systematically studies factors influencing privacy risk of trained ML models. This has significant positive impact on users training ML models on personal data by allowing them to understand and limit the risks.

**Reproducibility** We provide the code for reproducing the experiments in the supplementary material and will publish the code in an open repository after acceptance of the paper. All used pre-trained models and data sets are publicly available.

## Acknowledgements

This work was supported by the Research Council of Finland (Flagship programme: Finnish Center for Artificial Intelligence, FCAI, Grant 356499 and Grant 359111), the Strategic Research Council at the Research Council of Finland (Grant 358247) as well as the European Union (Project 101070617). Views and opinions expressed are however those of the author(s) only and do not necessarily reflect those of the European Union or the European Commission. Neither the European Union nor the granting authority can be held responsible for them. The authors wish to thank the Finnish Computing Competence Infrastructure (FCCI) for supporting this project with computational and data storage resources. We thank John F. Bronskill for helpful discussions regarding few-shot learning.

## References

- T. Akiba, S. Sano, T. Yanase, T. Ohta, and M. Koyama. Optuna: A next-generation hyperparameter optimization framework. In A. Teredesai, V. Kumar, Y. Li, R. Rosales, E. Terzi, and G. Karypis, editors, *Proceedings of the 25th ACM SIGKDD International Conference on Knowledge Discovery & Data Mining, KDD 2019, Anchorage, AK, USA, August 4-8, 2019*, pages 2623–2631. ACM, 2019. doi: 10.1145/3292500.3330701. URL <https://doi.org/10.1145/3292500.3330701>.
- B. Balle, G. Cherubin, and J. Hayes. Reconstructing training data with informed adversaries. In *43rd IEEE Symposium on Security and Privacy, SP 2022, San Francisco, CA, USA, May 22-26, 2022*, pages 1138–1156. IEEE, 2022. doi: 10.1109/SP46214.2022.9833677. URL <https://doi.org/10.1109/SP46214.2022.9833677>.
- J. Bergstra, R. Bardenet, Y. Bengio, and B. Kégl. Algorithms for hyper-parameter optimization. In J. Shawe-Taylor, R. S. Zemel, P. L. Bartlett, F. C. N. Pereira, and K. Q. Weinberger, editors, *Advances in Neural Information Processing Systems 24: 25th Annual Conference on Neural Information Processing Systems 2011. Proceedings of a meeting held 12-14 December 2011, Granada, Spain*, pages 2546–2554, 2011. URL <https://proceedings.neurips.cc/paper/2011/hash/86e8f7ab32cfd12577bc2619bc635690-Abstract.html>.
- N. Carlini, S. Chien, M. Nasr, S. Song, A. Terzis, and F. Tramèr. Membership inference attacks from first principles. In *43rd IEEE Symposium on Security and Privacy, SP 2022, San Francisco, CA, USA, May 22-26, 2022*, pages 1897–1914. IEEE, 2022. doi: 10.1109/SP46214.2022.9833649. URL <https://doi.org/10.1109/SP46214.2022.9833649>.
- D. Chen, N. Yu, Y. Zhang, and M. Fritz. GAN-leaks: A taxonomy of membership inference attacks against generative models. In J. Ligatti, X. Ou, J. Katz, and G. Vigna, editors, *CCS '20: 2020 ACM SIGSAC Conference on Computer and Communications Security, Virtual Event, USA, November 9-13, 2020*, pages 343–362. ACM, 2020. doi: 10.1145/3372297.3417238. URL <https://doi.org/10.1145/3372297.3417238>.
- G. Cheng, J. Han, and X. Lu. Remote sensing image scene classification: Benchmark and state of the art. *Proceedings of the IEEE*, 105(10):1865–1883, 2017.

- C. J. Clopper and E. S. Pearson. The use of confidence or fiducial limits illustrated in the case of the binomial. *Biometrika*, 26(4):404–413, Dec. 1934. doi: 10.1093/biomet/26.4.404. URL <https://doi.org/10.1093/biomet/26.4.404>.
- J. Dong, A. Roth, and W. J. Su. Gaussian differential privacy. *Journal of the Royal Statistical Society: Series B (Statistical Methodology)*, 84(1):3–37, 2022. doi: 10.1111/rssb.12454.
- A. Dosovitskiy, L. Beyer, A. Kolesnikov, D. Weissenborn, X. Zhai, T. Unterthiner, M. Dehghani, M. Minderer, G. Heigold, S. Gelly, J. Uszkoreit, and N. Houlsby. An image is worth 16x16 words: Transformers for image recognition at scale. In *9th International Conference on Learning Representations, ICLR 2021, Virtual Event, Austria, May 3-7, 2021*. OpenReview.net, 2021. URL <https://openreview.net/forum?id=YicbFdNTTy>.
- C. Dwork, F. McSherry, K. Nissim, and A. D. Smith. Calibrating noise to sensitivity in private data analysis. In S. Halevi and T. Rabin, editors, *Theory of Cryptography, Third Theory of Cryptography Conference, TCC 2006, New York, NY, USA, March 4-7, 2006, Proceedings*, volume 3876 of *Lecture Notes in Computer Science*, pages 265–284. Springer, 2006. doi: 10.1007/11681878\_14. URL [https://doi.org/10.1007/11681878\\_14](https://doi.org/10.1007/11681878_14).
- V. Feldman and T. Zrnic. Individual privacy accounting via a Rényi filter. In M. Ranzato, A. Beygelzimer, Y. N. Dauphin, P. Liang, and J. W. Vaughan, editors, *Advances in Neural Information Processing Systems 34: Annual Conference on Neural Information Processing Systems 2021, NeurIPS 2021, December 6-14, 2021, virtual*, pages 28080–28091, 2021. URL <https://proceedings.neurips.cc/paper/2021/hash/ec7f346604f518906d35ef0492709f78-Abstract.html>.
- P. Helber, B. Bischke, A. Dengel, and D. Borth. Eurosat: A novel dataset and deep learning benchmark for land use and land cover classification. *IEEE Journal of Selected Topics in Applied Earth Observations and Remote Sensing*, 12(7):2217–2226, 2019.
- H. Hu, Z. Salcic, L. Sun, G. Dobbie, P. S. Yu, and X. Zhang. Membership inference attacks on machine learning: A survey. *ACM Computing Surveys (CSUR)*, 54(11s):1–37, 2022.
- D. P. Kingma and J. Ba. Adam: A method for stochastic optimization. In Y. Bengio and Y. LeCun, editors, *3rd International Conference on Learning Representations, ICLR 2015, San Diego, CA, USA, May 7-9, 2015, Conference Track Proceedings*, 2015. URL <http://arxiv.org/abs/1412.6980>.
- A. Kolesnikov, L. Beyer, X. Zhai, J. Puigcerver, J. Yung, S. Gelly, and N. Houlsby. Big transfer (BiT): General visual representation learning. In A. Vedaldi, H. Bischof, T. Brox, and J. Frahm, editors, *Computer Vision - ECCV 2020 - 16th European Conference, Glasgow, UK, August 23-28, 2020, Proceedings, Part V*, volume 12350 of *Lecture Notes in Computer Science*, pages 491–507. Springer, 2020. doi: 10.1007/978-3-030-58558-7\_29. URL [https://doi.org/10.1007/978-3-030-58558-7\\_29](https://doi.org/10.1007/978-3-030-58558-7_29).
- A. Koskela, M. Tobaben, and A. Honkela. Individual privacy accounting with Gaussian differential privacy. In *The Eleventh International Conference on Learning Representations, ICLR 2023, Kigali, Rwanda, May 1-5, 2023*. OpenReview.net, 2023. URL [https://openreview.net/pdf?id=JmC\\_T1d3v-f](https://openreview.net/pdf?id=JmC_T1d3v-f).
- A. Krizhevsky. Learning multiple layers of features from tiny images. Master’s thesis, University of Toronto, 2009.
- M. Nasr, N. Carlini, J. Hayase, M. Jagielski, A. F. Cooper, D. Ippolito, C. A. Choquette-Choo, E. Wallace, F. Tramèr, and K. Lee. Scalable extraction of training data from (production) language models. *CoRR*, abs/2311.17035, 2023. doi: 10.48550/ARXIV.2311.17035. URL <https://doi.org/10.48550/arXiv.2311.17035>.
- G. D. Németh, M. A. Lozano, N. Quadrianto, and N. Oliver. Addressing membership inference attack in federated learning with model compression. *CoRR*, abs/2311.17750, 2023. doi: 10.48550/ARXIV.2311.17750.

- O. M. Parkhi, A. Vedaldi, A. Zisserman, and C. V. Jawahar. Cats and dogs. In *2012 IEEE Conference on Computer Vision and Pattern Recognition, Providence, RI, USA, June 16-21, 2012*, pages 3498–3505. IEEE Computer Society, 2012. doi: 10.1109/CVPR.2012.6248092. URL <https://doi.org/10.1109/CVPR.2012.6248092>.
- E. Perez, F. Strub, H. de Vries, V. Dumoulin, and A. C. Courville. Film: Visual reasoning with a general conditioning layer. In S. A. McIlraith and K. Q. Weinberger, editors, *Proceedings of the Thirty-Second AAAI Conference on Artificial Intelligence, (AAAI-18), the 30th innovative Applications of Artificial Intelligence (IAAI-18), and the 8th AAAI Symposium on Educational Advances in Artificial Intelligence (EAAI-18), New Orleans, Louisiana, USA, February 2-7, 2018*, pages 3942–3951. AAAI Press, 2018. URL <https://www.aaai.org/ocs/index.php/AAAI/AAAI18/paper/view/16528>.
- O. Russakovsky, J. Deng, H. Su, J. Krause, S. Satheesh, S. Ma, Z. Huang, A. Karpathy, A. Khosla, M. S. Bernstein, A. C. Berg, and L. Fei-Fei. ImageNet large scale visual recognition challenge. *Int. J. Comput. Vis.*, 115(3):211–252, 2015. doi: 10.1007/S11263-015-0816-Y. URL <https://doi.org/10.1007/s11263-015-0816-y>.
- S. Seabold and J. Perktold. statsmodels: Econometric and statistical modeling with python. In *9th Python in Science Conference*, 2010.
- R. Shokri, M. Stronati, C. Song, and V. Shmatikov. Membership inference attacks against machine learning models. In *2017 IEEE Symposium on Security and Privacy, SP 2017, San Jose, CA, USA, May 22-26, 2017*, pages 3–18. IEEE Computer Society, 2017. doi: 10.1109/SP.2017.41. URL <https://doi.org/10.1109/SP.2017.41>.
- A. Shysheya, J. Bronskill, M. Patacchiola, S. Nowozin, and R. E. Turner. FiT: parameter efficient few-shot transfer learning for personalized and federated image classification. In *The Eleventh International Conference on Learning Representations, ICLR 2023, Kigali, Rwanda, May 1-5, 2023*. OpenReview.net, 2023. URL <https://openreview.net/pdf?id=9aokcgbVIj1>.
- M. Tobaben, A. Shysheya, J. Bronskill, A. Pavard, S. Tople, S. Z. Béguelin, R. E. Turner, and A. Honkela. On the efficacy of differentially private few-shot image classification. *Transactions on Machine Learning Research*, 2023. ISSN 2835-8856. URL <https://openreview.net/forum?id=hFsr59Imzm>.
- B. S. Veeling, J. Linmans, J. Winkens, T. Cohen, and M. Welling. Rotation equivariant cnns for digital pathology. In *International Conference on Medical image computing and computer-assisted intervention*, pages 210–218. Springer, 2018.
- A. Yousefpour, I. Shilov, A. Sablayrolles, D. Testuggine, K. Prasad, M. Malek, J. Nguyen, S. Gosh, A. Bharadwaj, J. Zhao, G. Cormode, and I. Mironov. Opacus: User-friendly differential privacy library in PyTorch. *ArXiv preprint*, abs/2109.12298, 2021. URL <https://arxiv.org/abs/2109.12298>.
- D. Yu, G. Kamath, J. Kulkarni, T.-Y. Liu, J. Yin, and H. Zhang. Individual privacy accounting for differentially private stochastic gradient descent. *Transactions on Machine Learning Research*, 2023. ISSN 2835-8856. URL <https://openreview.net/forum?id=14Jcxs0fpC>.
- X. Zhai, J. Puigcerver, A. Kolesnikov, P. Ruysen, C. Riquelme, M. Lucic, J. Djolonga, A. S. Pinto, M. Neumann, A. Dosovitskiy, et al. A large-scale study of representation learning with the visual task adaptation benchmark. *ArXiv preprint*, abs/1910.04867, 2019. URL <https://arxiv.org/abs/1910.04867>.

## A Training details

### A.1 Parameterization

We utilise pre-trained feature extractors BiT-M-R50x1 (R-50) (Kolesnikov et al., 2020) with 23.5M parameters and Vision Transformer ViT-Base-16 (ViT-B) (Dosovitskiy et al., 2021) with 85.8M

parameters, both pretrained on the ImageNet-21K data set (Russakovsky et al., 2015). We download the feature extractor checkpoints from the respective repositories.

Following Tobaben et al. (2023) that show the favorable trade-off of parameter-efficient fine-tuning between computational cost, utility and privacy even for small data sets, we only consider fine-tuning subsets of all feature extractor parameters. We consider the following configurations:

- **Head:** We train a linear layer on top of the pre-trained feature extractor.
- **FiLM:** In addition to the linear layer from Head, we fine-tune parameter-efficient FiLM (Perez et al., 2018) adapters scattered throughout the network. While a diverse set of adapters has been proposed, we utilise FiLM as it has been shown to be competitive in prior work (Shysheya et al., 2023; Tobaben et al., 2023).

### A.1.1 Licenses and Access

The licenses and means to access the model checkpoints can be found below.

- BiT-M-R50x1 (R-50) (Kolesnikov et al., 2020) is licensed with the Apache-2.0 license and can be obtained through the instructions on <https://github.com/google-research/big-transfer>.
- Vision Transformer ViT-Base-16 (ViT-B) (Dosovitskiy et al., 2021) is licensed with the Apache-2.0 license and can be obtained through the instructions on [https://github.com/google-research/vision\\_transformer](https://github.com/google-research/vision_transformer).

## A.2 Hyperparameter tuning

Our hyperparameter tuning is heavily inspired by the comprehensive few-shot experiments by Tobaben et al. (2023). We utilise their hyperparameter tuning protocol as it has been proven to yield SOTA results for (DP) few-shot models. Given the input  $\mathcal{D}$  data set we perform hyperparameter tuning by splitting the  $\mathcal{D}$  into 70% train and 30% validation. We then perform the specified iterations of hyperparameter tuning using the tree-structured Parzen estimator (Bergstra et al., 2011) strategy as implemented in Optuna (Akiba et al., 2019) to derive a set of hyperparameters that yield the highest accuracy on the validation split. This set of hyperparameters is subsequently used to train all shadow models with the Adam optimizer Kingma and Ba (2015). Details on the set of hyperparameters that are tuned and their ranges can be found in Table A1.

Table A1: Hyperparameter ranges used for the Bayesian optimization with Optuna.

	lower bound	upper bound
batch size	10	$ \mathcal{D} $
clipping norm	0.2	10
epochs	1	200
learning rate	1e-7	1e-2

## A.3 Data sets

Table A2 shows the data sets used in the paper. We base our experiments on a subset of the few-shot benchmark VTAB (Zhai et al., 2019) that achieves a classification accuracy  $> 80\%$  and thus would be considered to be used by a practitioner. Additionally, we add CIFAR10 which is not part of the original VTAB benchmark.

### A.3.1 Licenses and Access

The licenses and means to access the data sets can be found below. We downloaded all data sets from TensorFlow datasets <https://www.tensorflow.org/datasets> but Resics45 which required manual download.

Table A2: Used datasets in the paper, their minimum and maximum shots  $S$  and maximum number of classes  $C$  and their test accuracy when fine-tuning a non-DP ViT-B Head. The test accuracy for EuroSAT and Resics45 is computed on the part of the training split that is not used for training the particular model due to both datasets missing an official test split. Note that LiRA requires  $2S$  for training the shadow models and thus  $S$  is smaller than when only performing fine-tuning.

dataset	(max.) $C$	min. $S$	max. $S$	test accuracy (min. $S$ )	test accuracy (max. $S$ )
Patch Camelyon (Veeling et al., 2018)	2	256	65536	82.8%	85.6%
CIFAR10 (Krizhevsky, 2009)	10	8	2048	92.7%	97.7%
EuroSAT (Helber et al., 2019)	10	8	512	80.2%	96.7%
Pets (Parkhi et al., 2012)	37	8	32	82.3%	90.7%
Resics45 (Cheng et al., 2017)	45	32	256	83.5%	91.6%
CIFAR100 (Krizhevsky, 2009)	100	16	128	82.2%	87.6%

- Patch Camelyon (Veeling et al., 2018) is licensed with Creative Commons Zero v1.0 Universal (cc0-1.0) and we use version 2.0.0 of the data set as specified on [https://www.tensorflow.org/datasets/catalog/patch\\_camelyon](https://www.tensorflow.org/datasets/catalog/patch_camelyon).
- CIFAR10 (Krizhevsky, 2009) is licensed with an unknown license and we use version 3.0.2 of the data set as specified on <https://www.tensorflow.org/datasets/catalog/cifar10>.
- EuroSAT (Helber et al., 2019) is licensed with MIT and we use version 2.0.0 of the data set as specified on <https://www.tensorflow.org/datasets/catalog/eurosat>.
- Pets (Parkhi et al., 2012) is licensed with CC BY-SA 4.0 Deed and we use version 3.2.0 of the data set as specified on [https://www.tensorflow.org/datasets/catalog/oxford\\_iiit\\_pet](https://www.tensorflow.org/datasets/catalog/oxford_iiit_pet).
- Resics45 (Cheng et al., 2017) is licensed with an unknown license and we use version 3.0.0 of the data set as specified on <https://www.tensorflow.org/datasets/catalog/resisc45>.
- CIFAR100 (Krizhevsky, 2009) is licensed with an unknown license and we use version 3.0.2 of the data set as specified on <https://www.tensorflow.org/datasets/catalog/cifar100>.

#### A.4 Compute Resources

All experiments but the R-50 (FiLM) experiments are run on CPU with 8 cores and 16 GB of host memory. The training time depends on the model (ViT is cheaper than R-50), number of shots  $S$  and the number of classes  $C$  but ranges for the training of one model from some minutes to an hour. This assumes that the images are passed once through the pre-trained backbone and then cached as feature vectors. The provided code implements this optimization.

In Section 5 we record the per-sample gradients during the training. This makes the training much more expensive despite the use of efficient per-sample gradient computation using Opacus Yousefpour et al. (2021). The training of the considered models does still not exceed one hour per model as we only consider settings with relatively low  $S$  for this part of the experiments.

The R-50 (FiLM) experiments are significantly more expensive and utilise a NVIDIA V100 with 40 GB VRAM, 10 CPU cores and 64 GB of host memory. The training of 257 shadow models then does not exceed 24h for the settings that we consider.

We estimate that in total we spend around 7 days of V100 and some dozens of weeks of CPU core time but more exact measurements are hard to make.

## B Additional results

In this section, we provide tabular results for our experiments and additional figures that did not fit into the main paper.

### B.1 Additional results for Section 3

This Section contains additional results for Section 3.

#### B.1.1 Vulnerability as a function of shots

This section displays additional results to Figure 1a for  $FPR \in \{0.1, 0.01, 0.001\}$  for ViT-B and R-50 in in Figure A.1 and Tables A3 and A4.

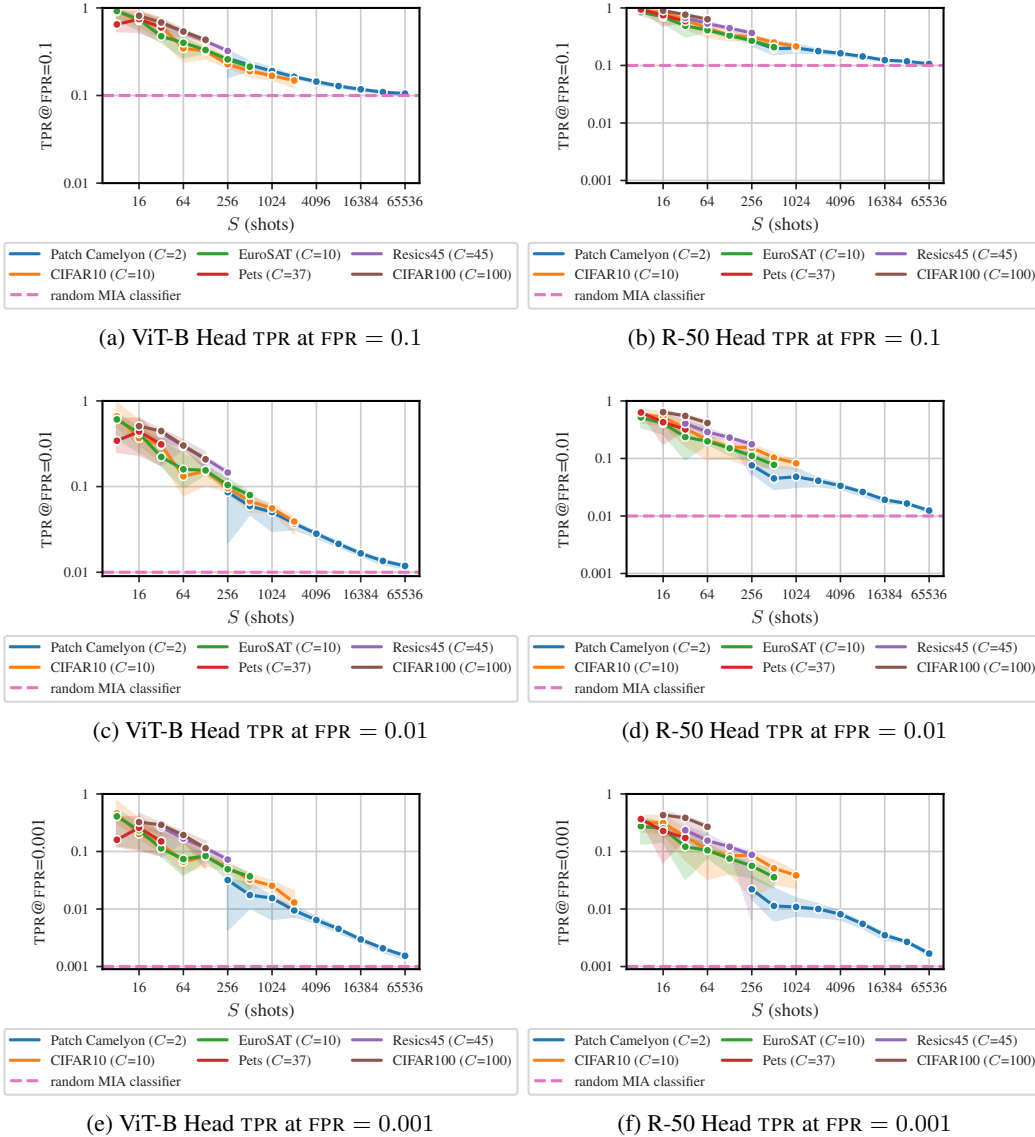


Figure A.1: MIA vulnerability as a function of shots (examples per class) when attacking a pre-trained ViT-B and R-50 Head trained without DP on different downstream data sets. The errorbars display the minimum and maximum Clopper-Pearson CIs over six seeds and the solid line the median.

Table A3: Median MIA vulnerability over six seeds as a function of  $S$  (shots) when attacking a Head trained without DP on-top of a ViT-B. The ViT-B is pre-trained on ImageNet-21k.

dataset	classes ( $C$ )	shots ( $S$ )	tpr@fpr=0.1	tpr@fpr=0.01	tpr@fpr=0.001
Patch Camelyon (Veeling et al., 2018)	2	256	0.266	0.086	0.032
		512	0.223	0.059	0.018
		1024	0.191	0.050	0.015
		2048	0.164	0.037	0.009
		4096	0.144	0.028	0.007
		8192	0.128	0.021	0.005
		16384	0.118	0.017	0.003
		32768	0.109	0.014	0.002
CIFAR10 (Krizhevsky, 2009)	10	65536	0.105	0.012	0.002
		8	0.910	0.660	0.460
		16	0.717	0.367	0.201
		32	0.619	0.306	0.137
		64	0.345	0.132	0.067
		128	0.322	0.151	0.082
		256	0.227	0.096	0.054
		512	0.190	0.068	0.032
EuroSAT (Helber et al., 2019)	10	1024	0.168	0.056	0.025
		2048	0.148	0.039	0.013
		8	0.921	0.609	0.408
		16	0.738	0.420	0.234
		32	0.475	0.222	0.113
		64	0.400	0.159	0.074
		128	0.331	0.155	0.084
		256	0.259	0.104	0.049
Pets (Parkhi et al., 2012)	37	512	0.213	0.080	0.037
		8	0.648	0.343	0.160
		16	0.745	0.439	0.259
Resics45 (Cheng et al., 2017)	45	32	0.599	0.311	0.150
		64	0.672	0.425	0.267
		128	0.531	0.295	0.168
CIFAR100 (Krizhevsky, 2009)	100	128	0.419	0.212	0.115
		256	0.323	0.146	0.072
		16	0.814	0.508	0.324
		32	0.683	0.445	0.290
		64	0.538	0.302	0.193
		128	0.433	0.208	0.114

Table A4: Median MIA vulnerability over six seeds as a function of  $S$  (shots) when attacking a Head trained without DP on-top of a R-50. The R-50 is pre-trained on ImageNet-21k.

dataset	classes ( $C$ )	shots ( $S$ )	tpr@fpr=0.1	tpr@fpr=0.01	tpr@fpr=0.001
Patch Camelyon (Veeling et al., 2018)	2	256	0.272	0.076	0.022
		512	0.195	0.045	0.011
		1024	0.201	0.048	0.011
		2048	0.178	0.041	0.010
		4096	0.163	0.033	0.008
		8192	0.143	0.026	0.006
		16384	0.124	0.019	0.004
		32768	0.118	0.016	0.003
		65536	0.106	0.012	0.002
CIFAR10 (Krizhevsky, 2009)	10	8	0.911	0.574	0.324
		16	0.844	0.526	0.312
		32	0.617	0.334	0.183
		64	0.444	0.208	0.106
		128	0.334	0.159	0.084
		256	0.313	0.154	0.086
		512	0.251	0.103	0.051
		1024	0.214	0.082	0.038
EuroSAT (Helber et al., 2019)	10	8	0.846	0.517	0.275
		16	0.699	0.408	0.250
		32	0.490	0.236	0.121
		64	0.410	0.198	0.105
		128	0.332	0.151	0.075
		256	0.269	0.111	0.056
		512	0.208	0.077	0.036
Pets (Parkhi et al., 2012)	37	8	0.937	0.631	0.366
		16	0.745	0.427	0.227
		32	0.588	0.321	0.173
Resics45 (Cheng et al., 2017)	45	32	0.671	0.405	0.235
		64	0.534	0.289	0.155
		128	0.445	0.231	0.121
		256	0.367	0.177	0.088
CIFAR100 (Krizhevsky, 2009)	100	16	0.897	0.638	0.429
		32	0.763	0.549	0.384
		64	0.634	0.414	0.269

### B.1.2 Vulnerability as a function of the number of classes

This section displays additional results to Figure 1b for  $FPR \in \{0.1, 0.01, 0.001\}$  for ViT-B and R-50 in in Figure A.2 and Tables A5 and A6.

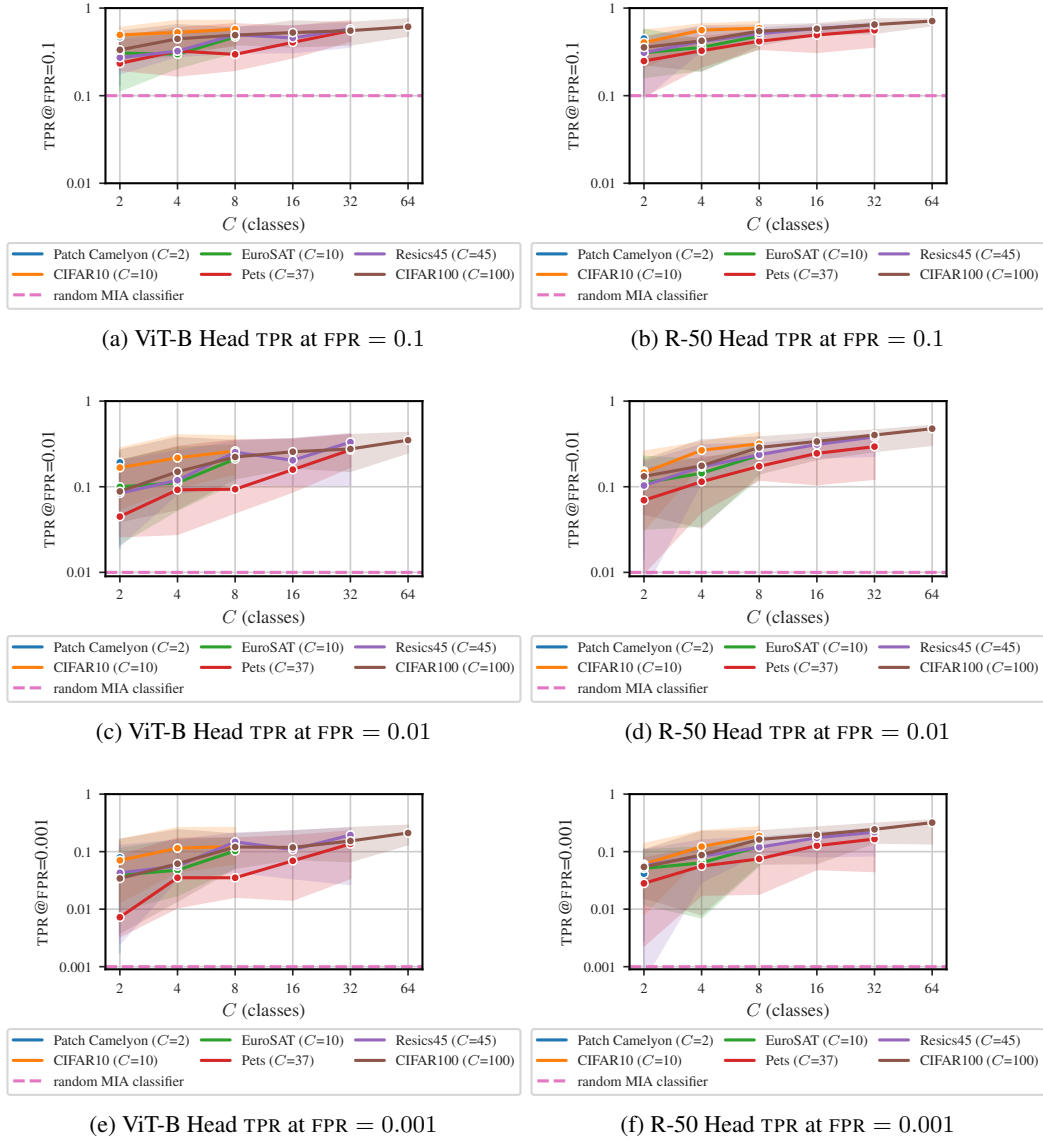


Figure A.2: MIA vulnerability as a function of  $C$  (classes) when attacking a ViT-B and R-50 Head fine-tuned without DP on different data sets where the classes are randomly sub-sampled and  $S = 32$ . The solid line displays the median and the errorbars the min and max clopper-pearson CIs over 12 seeds.

Table A5: Median MIA vulnerability over 12 seeds as a function of  $C$  (classes) when attacking a Head trained without DP on-top of a ViT-B. The ViT-B is pre-trained on ImageNet-21k.

dataset	shots ( $S$ )	classes ( $C$ )	tpr@fpr=0.1	tpr@fpr=0.01	tpr@fpr=0.001
Patch Camelyon (Veeling et al., 2018)	32	2	0.467	0.192	0.080
CIFAR10 (Krizhevsky, 2009)	32	2	0.494	0.167	0.071
		4	0.527	0.217	0.115
		8	0.574	0.262	0.123
EuroSAT (Helber et al., 2019)	32	2	0.306	0.100	0.039
		4	0.298	0.111	0.047
		8	0.468	0.211	0.103
Pets (Parkhi et al., 2012)	32	2	0.232	0.045	0.007
		4	0.324	0.092	0.035
		8	0.296	0.094	0.035
		16	0.406	0.158	0.069
		32	0.553	0.269	0.136
Resics45 (Cheng et al., 2017)	32	2	0.272	0.084	0.043
		4	0.322	0.119	0.056
		8	0.496	0.253	0.148
		16	0.456	0.204	0.108
		32	0.580	0.332	0.195
CIFAR100 (Krizhevsky, 2009)	32	2	0.334	0.088	0.035
		4	0.445	0.150	0.061
		8	0.491	0.223	0.121
		16	0.525	0.256	0.118
		32	0.553	0.276	0.153
		64	0.612	0.350	0.211

Table A6: Median MIA vulnerability over 12 seeds as a function of  $C$  (classes) when attacking a Head trained without DP on-top of a R-50. The R-50 is pre-trained on ImageNet-21k.

dataset	shots ( $S$ )	classes ( $C$ )	tpr@fpr=0.1	tpr@fpr=0.01	tpr@fpr=0.001
Patch Camelyon (Veeling et al., 2018)	32	2	0.452	0.151	0.041
CIFAR10 (Krizhevsky, 2009)	32	2	0.404	0.146	0.060
		4	0.560	0.266	0.123
		8	0.591	0.318	0.187
EuroSAT (Helber et al., 2019)	32	2	0.309	0.111	0.050
		4	0.356	0.144	0.064
		8	0.480	0.233	0.123
Pets (Parkhi et al., 2012)	32	2	0.249	0.068	0.029
		4	0.326	0.115	0.056
		8	0.419	0.173	0.075
		16	0.493	0.245	0.127
		32	0.559	0.294	0.166
Resics45 (Cheng et al., 2017)	32	2	0.310	0.103	0.059
		4	0.415	0.170	0.083
		8	0.510	0.236	0.119
		16	0.585	0.311	0.174
		32	0.644	0.382	0.218
CIFAR100 (Krizhevsky, 2009)	32	2	0.356	0.132	0.054
		4	0.423	0.176	0.087
		8	0.545	0.288	0.163
		16	0.580	0.338	0.196
		32	0.648	0.402	0.244
		64	0.711	0.476	0.320

### B.1.3 Data for FiLM and from scratch training

Table A7: MIA vulnerability data used in Figure 3b. Note that the data from Carlini et al. (2022) is only partially tabular, thus we estimated the TPR at FPR from the plots in the Appendix of their paper.

model	dataset	classes ( $C$ )	shots ( $S$ )	source	tpr@ fpr=0.1	tpr@ fpr=0.01	tpr@ fpr=0.001
R-50 FiLM	CIFAR10 (Krizhevsky, 2009)	10	50	This work	0.482	0.275	0.165
	CIFAR100 (Krizhevsky, 2009)	100	10	Tobaben et al. (2023)	0.933	0.788	0.525
			25	Tobaben et al. (2023)	0.766	0.576	0.449
			50	Tobaben et al. (2023)	0.586	0.388	0.227
			100	Tobaben et al. (2023)	0.448	0.202	0.077
	EuroSAT (Helber et al., 2019)	10	8	This work	0.791	0.388	0.144
	Patch Camelyon (Veeling et al., 2018)	2	256	This work	0.379	0.164	0.076
	Pets (Parkhi et al., 2012)	37	8	This work	0.956	0.665	0.378
Resics45 (Cheng et al., 2017)	45	32	This work	0.632	0.379	0.217	
from scratch (wide ResNet)	CIFAR10 (Krizhevsky, 2009)	10	2500	Carlini et al. (2022)	0.300	0.110	0.084
	CIFAR100 (Krizhevsky, 2009)	100	250	Carlini et al. (2022)	0.700	0.400	0.276

### B.1.4 Predicting data set vulnerability as function of $S$ and $C$

This section provides additional results for the model based on Equation (2)

Table A8: Results for fitting Equation (A1) with statsmodels Seabold and Perktold (2010) to ViT Head data at  $FPR \in \{0.1, 0.01, 0.001, 0.0001, 0.00001\}$ . We utilize an ordinary least squares. The test  $R^2$  assesses the fit to the data of R-50 Head.

coeff.	FPR	$R^2$	test $R^2$	coeff. value	std. error	$t$	$p >  z $	coeff. [0.025	coeff. 0.975]
$\beta_S$ (for $S$ )	0.1	0.952	0.907	-0.506	0.011	-44.936	0.000	-0.529	-0.484
	0.01	0.946	0.854	-0.555	0.014	-39.788	0.000	-0.582	-0.527
	0.001	0.930	0.790	-0.627	0.019	-32.722	0.000	-0.664	-0.589
	0.0001	0.852	0.618	-0.741	0.035	-21.467	0.000	-0.809	-0.673
	0.00001	0.837	0.404	-0.836	0.045	-18.690	0.000	-0.924	-0.748
	$\beta_C$ (for $C$ )	0.1	0.952	0.907	0.090	0.021	4.231	0.000	0.048
0.01		0.946	0.854	0.182	0.026	6.960	0.000	0.131	0.234
0.001		0.930	0.790	0.300	0.036	8.335	0.000	0.229	0.371
0.0001		0.852	0.618	0.363	0.065	5.616	0.000	0.236	0.491
0.00001		0.837	0.404	0.569	0.085	6.655	0.000	0.400	0.737
$\beta_0$ (intercept)		0.1	0.952	0.907	0.314	0.045	6.953	0.000	0.225
	0.01	0.946	0.854	0.083	0.056	1.491	0.137	-0.027	0.193
	0.001	0.930	0.790	-0.173	0.077	-2.261	0.025	-0.324	-0.022
	0.0001	0.852	0.618	-0.303	0.138	-2.202	0.029	-0.575	-0.032
	0.00001	0.837	0.404	-0.615	0.180	-3.414	0.001	-0.970	-0.260

Figure A.3 shows the performance for all considered FPR.

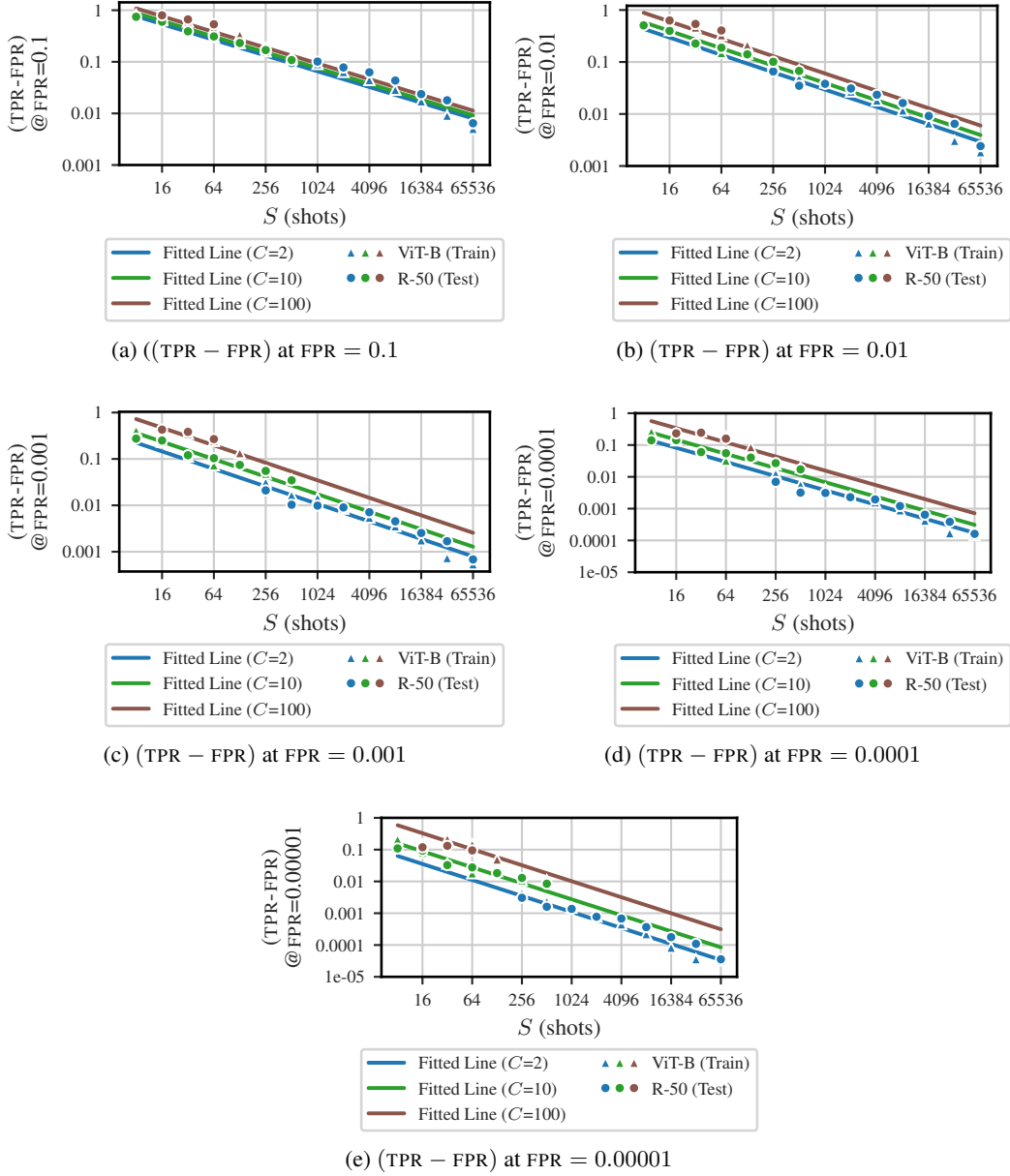


Figure A.3: Predicted MIA vulnerability as a function of  $S$  (shots) using a model based on Equation (2) fitted Table A3 (ViT-B). The triangles show the median TPR for the train set (ViT-B; Table A3) and circle the test set (R-50; Table A4) over six seeds. Note that the triangles and dots for  $C = 10$  are for EuroSAT.

## B.2 Simpler variant of the prediction model

The prediction model in the main text (Equation (2)) avoids predicting  $\text{TPR} < \text{FPR}$  in the tail when  $S$  is very large. In this section, we analyse a variation of the regression model that is simpler and predicts  $\log_{10}(\text{TPR})$  instead of  $\log_{10}(\text{TPR} - \text{FPR})$ . This variation fits worse to the empirical data and will predict  $\text{TPR} < \text{FPR}$  for high  $S$ .

The general form this variant can be found in Equation (A1), where  $\beta_S, \beta_C$  and  $\beta_0$  are the learnable regression parameters.

$$\log_{10}(\text{TPR}) = \beta_S \log_{10}(S) + \beta_C \log_{10}(C) + \beta_0 \tag{A1}$$

Table A9 provides tabular results on the performance of the variant.

Table A9: Results for fitting Equation (A1) with statsmodels Seabold and Perktold (2010) to ViT Head data at  $\text{FPR} \in \{0.1, 0.01, 0.001, 0.0001, 0.00001\}$ . We utilize an ordinary least squares. The test  $R^2$  assesses the fit to the data of R-50 Head.

coeff.	FPR	$R^2$	test $R^2$	coeff. value	std. error	$t$	$p >  z $	coeff. [0.025	coeff. 0.975]
$\beta_S$ (for $S$ )	0.1	0.908	0.764	-0.248	0.008	-30.976	0.000	-0.264	-0.233
	0.01	0.940	0.761	-0.416	0.011	-36.706	0.000	-0.438	-0.393
	0.001	0.931	0.782	-0.553	0.017	-32.507	0.000	-0.586	-0.519
	0.0001	0.865	0.628	-0.697	0.031	-22.274	0.000	-0.758	-0.635
	0.00001	0.862	0.400	-0.802	0.040	-20.311	0.000	-0.880	-0.725
$\beta_C$ (for $C$ )	0.1	0.908	0.764	0.060	0.015	3.955	0.000	0.030	0.089
	0.01	0.940	0.761	0.169	0.021	7.941	0.000	0.127	0.211
	0.001	0.931	0.782	0.297	0.032	9.303	0.000	0.234	0.360
	0.0001	0.865	0.628	0.371	0.059	6.328	0.000	0.255	0.486
	0.00001	0.862	0.400	0.580	0.076	7.679	0.000	0.431	0.729
$\beta_0$ (intercept)	0.1	0.908	0.764	0.029	0.032	0.913	0.362	-0.034	0.093
	0.01	0.940	0.761	-0.118	0.045	-2.613	0.010	-0.208	-0.029
	0.001	0.931	0.782	-0.295	0.068	-4.345	0.000	-0.429	-0.161
	0.0001	0.865	0.628	-0.387	0.125	-3.104	0.002	-0.633	-0.141
	0.00001	0.862	0.400	-0.683	0.159	-4.288	0.000	-0.996	-0.369

Figure A.4 plots the performance of the variant similar to Figure 3a in the main text.

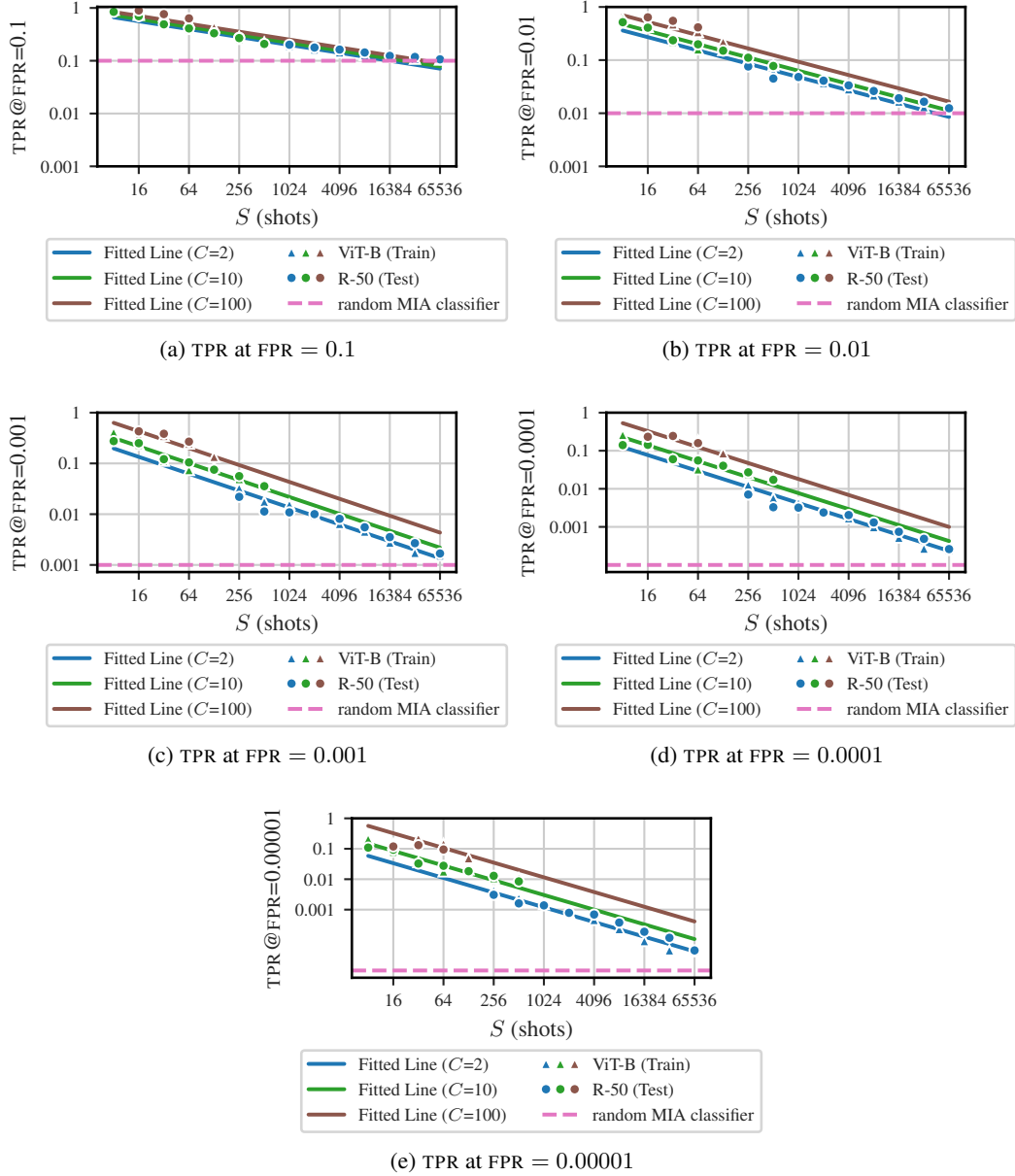


Figure A.4: Predicted MIA vulnerability as a function of  $S$  (shots) using a model based on Equation (A1) fitted Table A3 (ViT-B). The triangles show the median TPR for the train set (ViT-B; Table A3) and circle the test set (R-50; Table A4) over six seeds. Note that the triangles and dots for  $C = 10$  are for EuroSAT.

### B.3 Additional results for Section 4

This section provides additional results for Section 4.

### B.4 Rates of In- and Out-distribution Parameters as Function of data set Properties

LiRA assumes the attacker can build Gaussian distributions of losses for each data point  $x$  through the training of shadow models (see Section 2). We denote the distributions as following:

- *In-distribution*: Distribution of the losses of shadow models using  $x$  for training ( $x \in \mathcal{D}$ )
- *Out-distribution*: Distribution of the losses of shadow models *not* using  $x$  for training ( $x \notin \mathcal{D}$ )

In Figure A.5 we visualise the changes of the two distributions as functions of  $S$  and  $C$ .

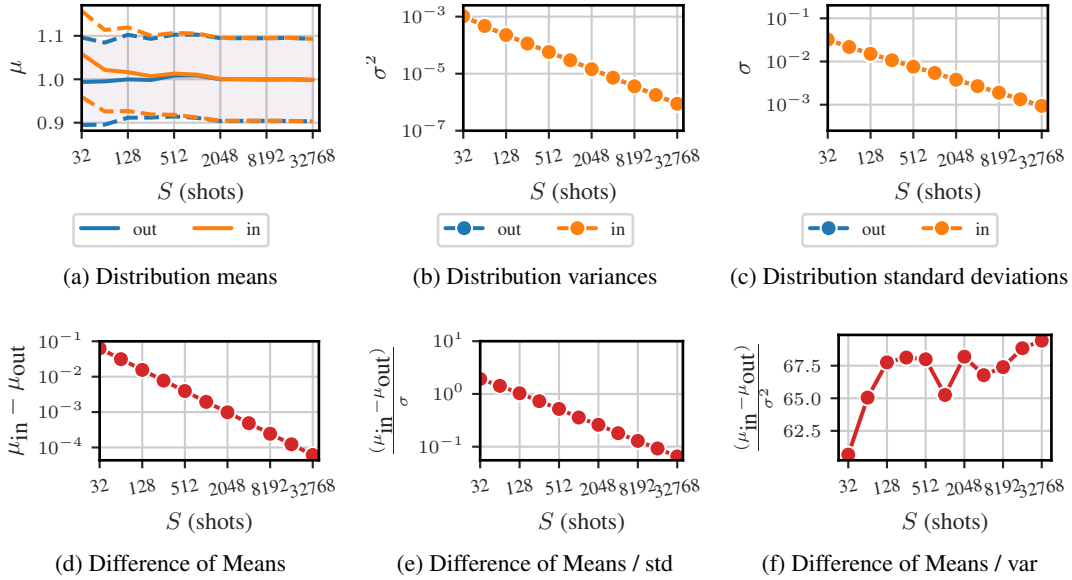


Figure A.5: Means of observed statistics of the in- and out-distributions for the simplified model with in-class  $\sigma = 0.1$ . The statistics are obtained for  $C = 2$ .

## B.5 Additional results for Section 5

This section provides additional results for Section 5. Figures A.6 and A.7 provide additional data for all considered FPR and for both ViT-B (Head) and R-50 (Head). Table A.10 the  $R^2$  scores for ViT-B (Head) and the experiment settings for ViT-B (Head) and R-50 (Head). Figure A.8 the relative  $R^2$  scores for R-50 (Head).

### B.5.1 MIA vulnerability as a function of individual gradient norms

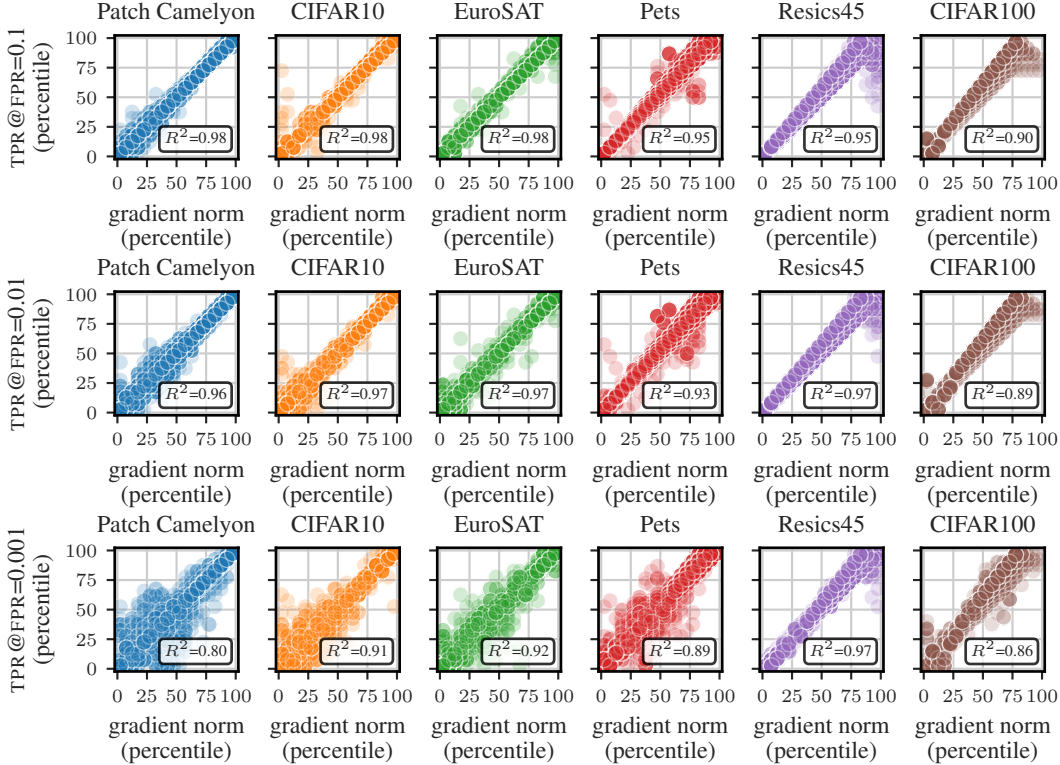


Figure A.6: ViT-B (Head): MIA vulnerability (TPR at FPR; percentiles among a seed) as a function of individual gradient norms (binned among a seed). The results have been obtained over six seeds. The number in the bottom right is the  $R^2$  (coefficient of determination) score when comparing the observed relationship between TPR at FPR and individual gradient norms to a scenario where individual gradient norms are a perfect predictor of individual MIA vulnerability (corresponding to a scenario where all points are on the diagonal line).

Table A.10: ViT-B (Head):  $R^2$  (coefficient of determination) score when comparing the observed relationship between TPR at FPR and individual gradient norms to a scenario where individual gradient norms are a perfect predictor of individual MIA vulnerability (corresponding to a scenario where all points are on the diagonal line).

dataset	shots ( $S$ )	classes ( $C$ )	data set size ( $ \mathcal{D} $ )	$R^2$ at FPR=0.1	$R^2$ at FPR=0.01	$R^2$ at FPR=0.001
Patch Camelyon (Veeling et al., 2018)	256	2	512	0.98	0.97	0.81
CIFAR10 (Krizhevsky, 2009)	64	10	640	0.98	0.98	0.92
EuroSAT (Helber et al., 2019)	64	10	640	0.98	0.97	0.92
Pets (Parkhi et al., 2012)	32	37	1184	0.95	0.93	0.89
Resics45 (Cheng et al., 2017)	32	45	1440	0.95	0.97	0.97
CIFAR100 (Krizhevsky, 2009)	16	100	1600	0.89	0.89	0.86

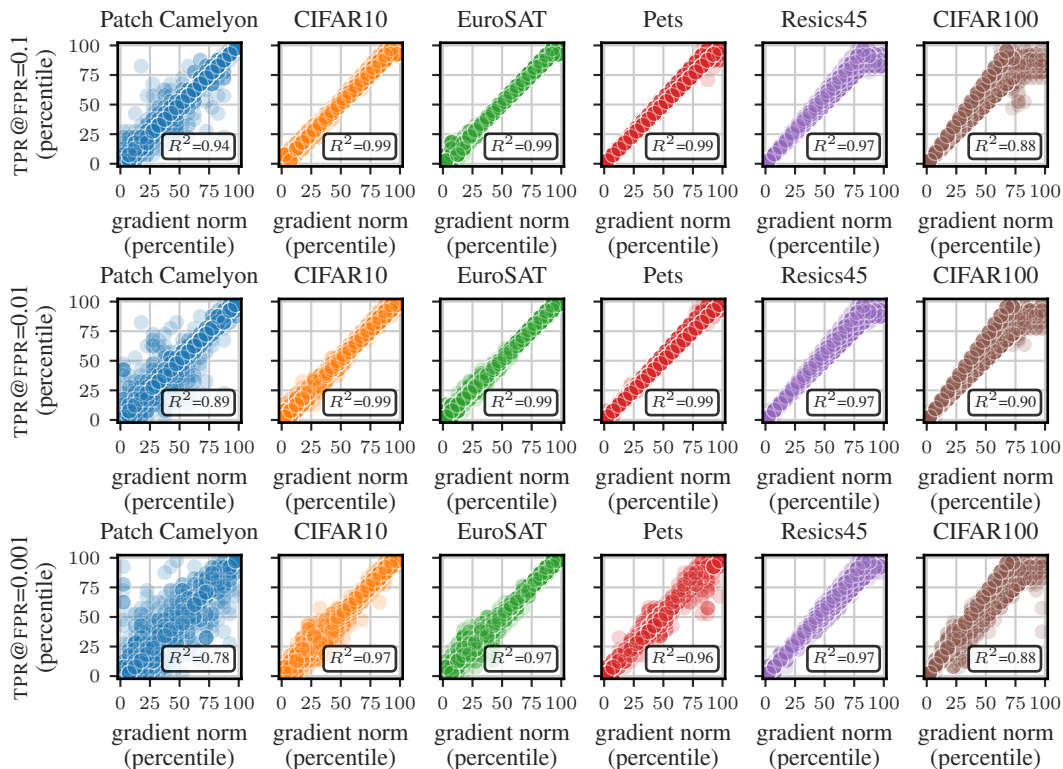


Figure A.7: R-50 (Head): MIA vulnerability (TPR at FPR; percentiles among a seed) as a function of individual gradient norms (binned among a seed). The results have been obtained over six seeds. The number in the bottom right is the  $R^2$  (coefficient of determination) score when comparing the observed relationship between TPR at FPR and individual gradient norms to a scenario where individual gradient norms are a perfect predictor of individual MIA vulnerability (corresponding to a scenario where all points are on the diagonal line).

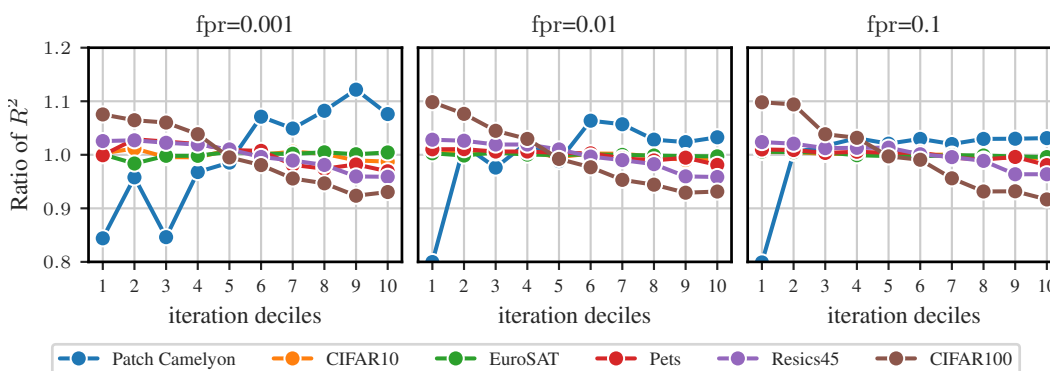


Figure A.8: R-50 (Head): Ratio between  $R^2$  per iteration decile and  $R^2$  over the whole training. A ratio  $> 1$  means that the decile is as more predictive than whole trace and a ratio  $< 1$  means that it is less predictive.

## B.5.2 MIA vulnerability as a function of feature space distance

This section provides additional data regarding the individual MIA prediction using feature space distances.

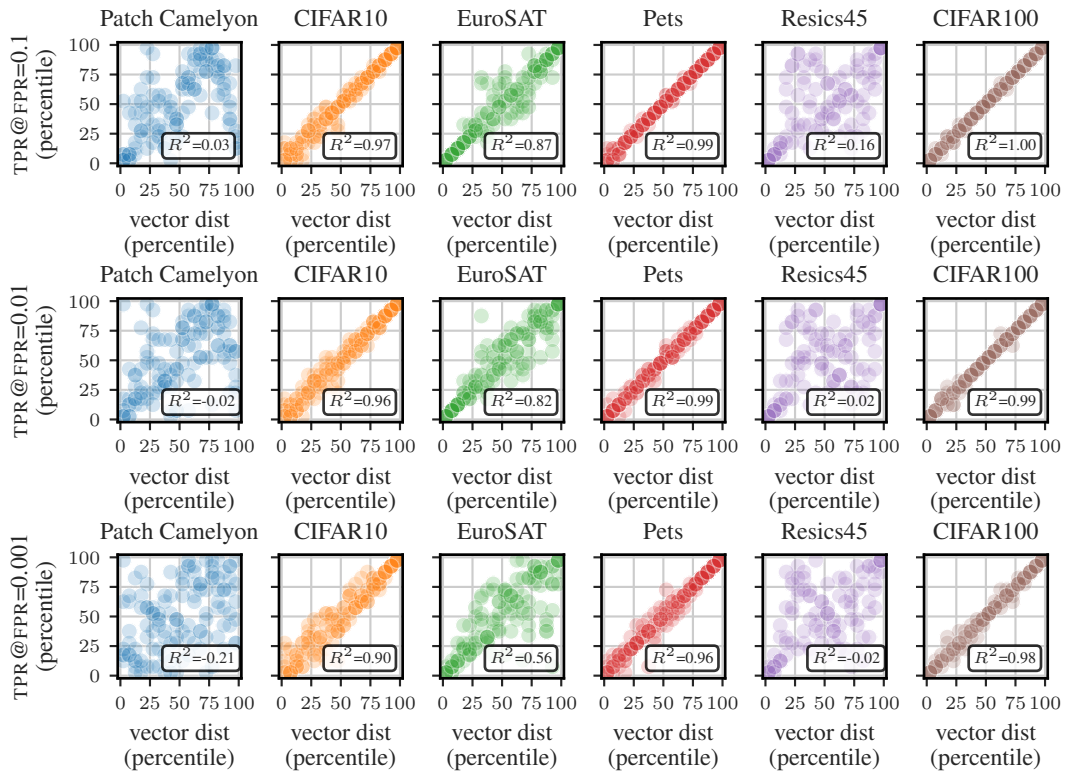


Figure A.9: ViT-B (Head): MIA vulnerability (TPR at FPR; percentiles among a seed) as a function of feature space distance (binned among a seed). The results have been obtained over six seeds.

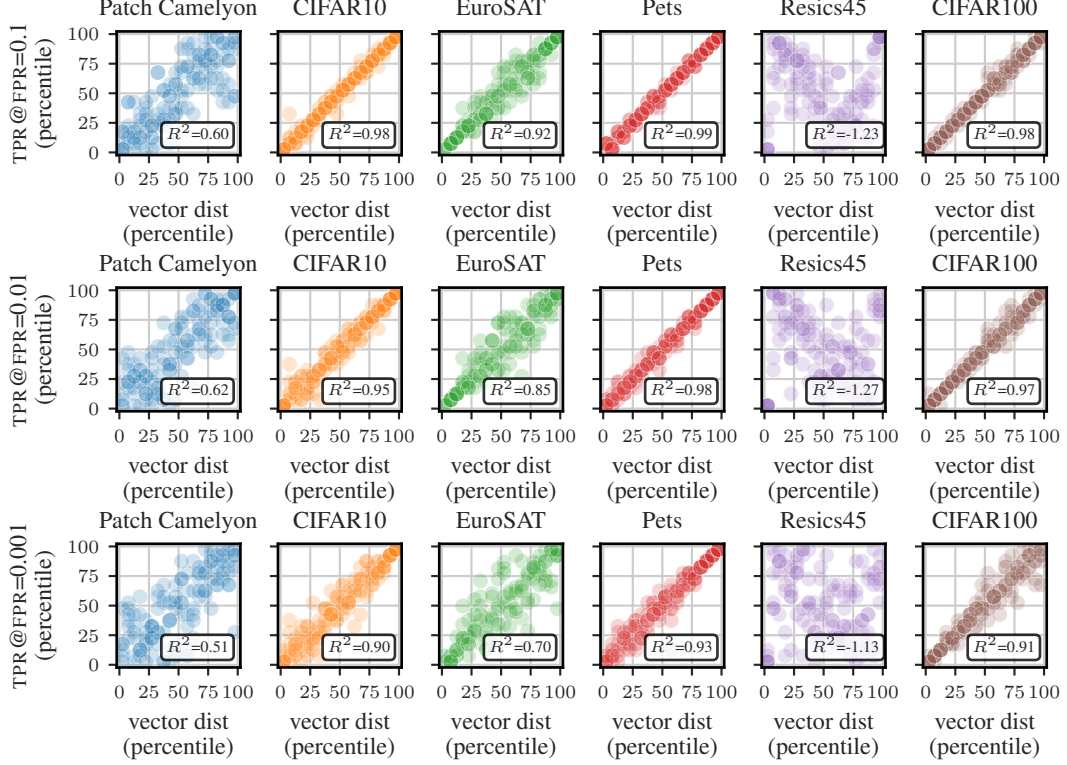


Figure A.10: R-50 (Head): MIA vulnerability (TPR at FPR; percentiles among a seed) as a function of feature space distance (binned among a seed). The results have been obtained over six seeds.

## C Missing proofs of Section 4.2

**Lemma 1.** *In the limit of infinite shadow models and with large enough  $S$ , the LiRA test statistics  $\lambda_{\text{FPR}}$  and  $\lambda_{\text{TPR}}$  obtain the following forms*

$$\lambda_{\text{FPR}} = -\frac{1}{2s^2\|x\|^2} \langle x, x - m_y \rangle \left( \frac{2s}{\sqrt{S}} \langle x, z \rangle + \frac{1}{S} \langle x, x - m_y \rangle \right) \quad (8)$$

$$\lambda_{\text{TPR}} \approx -\frac{1}{2s^2\|x\|^2} \langle x, x - m_y \rangle \left( \frac{2s}{\sqrt{S}} \langle x, z \rangle - \frac{2}{S} \|x\|^2 + \frac{1}{S} \langle x, x - m_y \rangle \right), \quad (9)$$

where  $z \sim \mathcal{N}(0, I_d)$ .

*Proof.* Recall

$$\text{FPR} = \Pr \left( \underbrace{-\frac{1}{2\sigma^2} (\mu_{\text{in}} - \mu_{\text{out}}) [-2t_x + (\mu_{\text{in}} + \mu_{\text{out}})]}_{\lambda_{\text{FPR}}} > \tau \mid x \notin \mathcal{D}_{\text{target}} \right) \quad (\text{A2})$$

$$\text{TPR} = \Pr \left( \underbrace{-\frac{1}{2\sigma^2} (\mu_{\text{in}} - \mu_{\text{out}}) [-2t_x + (\mu_{\text{in}} + \mu_{\text{out}})]}_{\lambda_{\text{TPR}}} > \tau \mid x \in \mathcal{D}_{\text{target}} \right). \quad (\text{A3})$$

We denote the class means for the  $m$ th in/out shadow data sets with  $r_{y,m}^{(\text{in})}$  and  $r_{y,m}^{(\text{out})}$

$$r_{y,m}^{(\text{in})} = \frac{1}{S} \left( \sum_{i=1}^{S-1} x_{i,m,y} + x \right), \quad r_{y,m}^{(\text{out})} = \frac{1}{S} \left( \sum_{i=1}^S x_{i,m,y} \right), \quad (\text{A4})$$

where  $x_{i,m,y}$  denotes the  $i$ th element of the  $m$ th shadow data set with label  $y$ . The corresponding scores  $s_{y,m}^{(\text{in})} = \langle x, r_{y,m}^{(\text{in})} \rangle$  and  $s_{y,m}^{(\text{out})} = \langle x, r_{y,m}^{(\text{out})} \rangle$  which can be written as

$$s_{y,m}^{(\text{in})} = \frac{1}{S} \left( \langle x, \sum_{i=1}^{S-1} x_{i,m,y} \rangle + \langle x, x \rangle \right) = \frac{1}{S} \left( \langle x, \sum_{i=1}^S x_{i,m,y} \rangle + \langle x, x - x_{S,m,y} \rangle \right) \quad (\text{A5})$$

$$s_{y,m}^{(\text{out})} = \frac{1}{S} \left( \langle x, \sum_{i=1}^S x_{i,m,y} \rangle \right) \quad (\text{A6})$$

Now, assuming we have arbitrarily many shadow models, we can write the LiRA statistics as

$$\mu_{\text{in}} = \mathbb{E}_{D_m}[s_{y,m}^{(\text{in})}], \quad \mu_{\text{out}} = \mathbb{E}_{D_m}[s_{y,m}^{(\text{out})}] = \langle x, m_y \rangle \quad (\text{A7})$$

$$\Rightarrow \mu_{\text{in}} - \mu_{\text{out}} = \frac{1}{S} \langle x, x - \mathbb{E}_{D_m}[x_{S,m}] \rangle = \frac{1}{S} \langle x, x - m_y \rangle, \quad (\text{A8})$$

where  $m_y$  is the true center of the  $y$ th cluster. For  $\sigma$  we have

$$\sigma^2 = \text{Var}(s_{y,m}^{(\text{out})}) \quad (\text{A9})$$

$$= \frac{1}{S^2} \sum_{i=1}^S \text{Var}(\langle x, x_{i,m} \rangle) \quad (\text{A10})$$

$$= \frac{1}{S} \text{Var}(\langle x, x_m^{(j)} \rangle) \quad (\text{A11})$$

$$= \frac{1}{S} \text{Var}(x_m^{(j)}) \|x\|^2 = \frac{1}{S} s^2 \|x\|^2, \quad (\text{A12})$$

where  $x_m^{(j)}$  denotes the  $j$ th dimension of the vector  $x_m$  and  $s$  is the std of each dimension of  $x_m$ . Now we can write the  $\lambda_{\text{FPR}}$  as

$$\lambda_{\text{FPR}} = -\frac{1}{2s^2 \|x\|^2} \langle x, x - m_y \rangle \left( -2t_x + 2\langle x, m_y \rangle + \frac{1}{S} \langle x, x - m_y \rangle \right). \quad (\text{A13})$$

In the FPR case, we have that  $x \notin \mathcal{D}_{\text{target}}$ , therefore for the  $t_x$  we have

$$t_x = \langle x, r_y^{(\text{target})} \rangle \sim \langle x, m_y \rangle + \frac{s}{\sqrt{S}} \langle x, z \rangle, \quad (\text{A14})$$

where  $z \sim N(0, I_d)$ . Substituting this into  $\lambda_{\text{FPR}}$  we have

$$\lambda_{\text{FPR}} = -\frac{1}{2s^2 \|x\|^2} \langle x, x - m_y \rangle \left( \frac{2s}{\sqrt{S}} \langle x, z \rangle + \frac{1}{S} \langle x, x - m_y \rangle \right). \quad (\text{A15})$$

We see that  $\lambda_{\text{FPR}}$  evolves as  $O(1/\sqrt{S})$ .

Next, we will focus on the  $\lambda_{\text{TPR}}$ . The expression remains otherwise the same as for  $\lambda_{\text{FPR}}$ , but since  $x \in \mathcal{D}_{\text{target}}$  the  $t_x$  changes to

$$t_x \sim \langle x, m_y \rangle + \frac{1}{S} \langle x, x \rangle + s \frac{1}{\sqrt{S}} \sqrt{1 - \frac{1}{S}} \langle x, z \rangle. \quad (\text{A16})$$

Hence, for large enough  $S$  we have

$$\lambda_{\text{TPR}} \approx -\frac{1}{2s^2 \|x\|^2} \langle x, x - m_y \rangle \left( \frac{2s}{\sqrt{S}} \langle x, z \rangle - \frac{2}{S} \|x\|^2 + \frac{1}{S} \langle x, x - m_y \rangle \right). \quad (\text{A17})$$

□